

CGPG-97/4-3
 U.Parma UPRF 97-04
 gr-qc/9703090

Matrix Elements of Thiemann's Hamiltonian Constraint in Loop Quantum Gravity

Roumen Borissov [†] ^{||}, Roberto De Pietri [‡] [¶] and Carlo Rovelli [§] [‡] [‡]

[†] Center for Gravitational Physics and Geometry, The Pennsylvania State University, University Park, PA 16802, USA.

[‡] Dipartimento Di Fisica, Università di Parma and I.N.F.N. Gruppo Collegato di Parma, I-43100 Parma, Europe.

[§] Department of Physics and Astronomy, University of Pittsburgh, Pittsburgh, PA 15260, USA;

Erwin Schrödinger Institute, A-1090 Vienna, Europe.

Abstract.

We present an explicit computation of matrix elements of the hamiltonian constraint operator in non-perturbative quantum gravity. In particular, we consider the euclidean term of Thiemann's version of the constraint and compute its action on trivalent states, for all its natural orderings. The calculation is performed using graphical techniques from the recoupling theory of colored knots and links. We exhibit the matrix elements of the hamiltonian constraint operator in the spin network basis in compact algebraic form.

PACS numbers: 04.60.-m, 02.70.-c, 04.60.Ds, 03.70+k

Short title: Matrix elements of Thiemann's Hamiltonian

October 2, 2018

^{||} E-mail address: borissov@phys.psu.edu

[¶] E-mail address: depietri@pr.infn.it

[‡] E-mail address: roveli@pitt.edu

1. Introduction

In general relativity, the local dynamics of the gravitational field is governed by a constraint rather than by a hamiltonian [1]. Accordingly, in non-perturbative quantum gravity the quantum dynamics is governed by a constraint operator [2], usually denoted the “hamiltonian constraint operator” (HCO) or the Wheeler-DeWitt operator. The construction and the analysis of this operator is a central problem in quantum gravity. For a long time, only formal or seriously ill-defined versions of the HCO were known. Concrete computations were thus impossible beyond semiclassical or minisuperspace approximations, and a predictive theory of the non-perturbative quantum dynamics of gravity was consequently lacking.

The situation is perhaps improving with the development of the loop version of non-perturbative quantum gravity [3], derived from the introduction of the Sen-Ashtekar variables [4, 5] (now evolved into the real Barbero variables [6, 7]). This approach, denoted “loop quantum gravity”, has provided a rigorous framework for describing quantum geometry (for recent reviews, and complete references see [8, 9, 10]). As far as kinematics is concerned, the approach has yielded striking predictions: in particular, geometric operators corresponding to volumes and areas have been shown to have computable discrete spectra. This result was first obtained by Rovelli and Smolin in [11] and later re-derived and sharpened with various alternative techniques ([12, 13, 14]; see [15] and references therein); its physical significance was first asserted in [16].

As far as dynamics is concerned, an extensive array of investigations of the HCO, starting from the pioneering work of Jacobson and Smolin [17] and continuing in [3, 18, 19, 20, 21], has recently culminated with the construction, due to Thiemann, of a mathematically well-defined operator [22]. This construction is already being used in various directions of research, for instance in the search for exact solutions to the constraints [23], or as a key ingredient of a spacetime formulation of the theory [24, 25]. In this last context, the matrix elements of the HCO play a role analogous to the coefficients of the vertices in the Feynmann diagrams. Modifications of the operator have been considered in [26].

Thiemann’s operator, however, is defined in a rather involved manner: its matrix elements and explicit action are far from easy to evaluate. This difficulty obstructs the research directions mentioned and renders the analysis of the operator quite difficult. In this work, we address this difficulty directly by studying Thiemann’s operator in detail, and showing how its matrix elements can be computed explicitly.

To perform the computation, we take advantage of two key techniques. First, we work in the spin network basis, introduced in quantum gravity in [27, 28], and fully developed in [29] (see [30] for an interesting historical reconstruction of these developments). Second, we use the technique developed in [9], based on the (Kauffman-Lins) tangle theoretical version of recoupling theory [31] (whose utility for quantum gravity was first suggested in [32]). Since Thiemann’s operator is gauge invariant but is defined in terms of gauge non-invariant operators, we extend here these techniques to gauge non-invariant states [33, 34].

Furthermore, we take full advantage of the complete equivalence between the “loop representation” [3, 9] and the “connection representation” [35, 36, 22] of loop quantum gravity (proven in detail in [37]; see also [15, 33]). It is this equivalence that allows us, for example, to use graphical calculus in a rigorous way in dealing with states that are functions of generalized connections.

We study here only the euclidean term of the HCO, but we expect that the techniques we use can be extended to the lorentzian term as well. Also, we restrict our attention to trivalent vertices: extension to any valence is straightforward. Thiemann defines two versions of the HCO: symmetric and non-symmetric. Here, we consider both operators, and show that they exhaust all “natural” orderings of the constraint.

We do not discuss the physical correctness of Thiemann’s operator. In particular, we do not address the objections that have been raised against it, concerning for instance the state dependence of the regularization, the strong commutativity (which shows consistency, but seems to fail to reproduce the classical constraint algebra [38]) or the possible need for adding terms to the operator suggested for instance in [26, 24]. Rather, we simply study the operator as defined by Thiemann, and show how its matrix elements can be computed, using recoupling theory. This analysis is likely to be needed before attempting a physical evaluation and, in any case, it is relevant even if modifications to the Thiemann operator are to be made.

In section 2 we define the mathematical framework. In particular, we discuss the generalization of the spin networks to the gauge non-invariant case. In section 3 we show in detail why graphical methods can be used in the present context, following [37]. Section 4 reviews Thiemann’s construction of the hamiltonian constraint. Section 5 presents our main calculations. For completeness, we have included three appendices: A discussion of the volume operator (Appendix A); technical details on the application of the graphical calculus in the context of the connection representation (Appendix B); and the basic formulae and concepts of recoupling theory (Appendix C).

2. Loop quantum gravity.

We start with a 4-manifold \mathcal{M} diffeomorphic to $\Sigma \times R$, where Σ is a compact 3-manifold. The classical phase space of general relativity can be taken as the space of the canonical pairs (A_a^i, \tilde{E}_i^a) of smooth fields over Σ . A_a^i is a connection 1-form on Σ taking values in the Lie algebra of $SU(2)$. Its conjugate momentum \tilde{E}_i^a is a vector density of weight one on Σ which takes values in the dual of $su(2)$. We use the dimensional constants

$$G = \frac{16\pi G_{\text{Newton}}}{c^3},$$

$$l_0^2 = \hbar G = 16\pi l_{\text{Planck}}^2 = \frac{16\pi \hbar G_{\text{Newton}}}{c^3},$$

where G_{Newton} is Newton’s gravitational constant and l_{Planck} is the Planck’s length. The fundamental Poisson bracket is:

$$\{A_a^i(x), \tilde{E}_j^b(y)\} = G \delta_j^i \delta_a^b \delta^3(x, y). \quad (2.1)$$

The canonical variables are subject to three sets of constraints – the $SU(2)$ Gauss constraint, the diffeomorphism constraint and the hamiltonian constraint. The space \mathcal{A} of the $SU(2)$ connections on Σ is the classical configuration space of general relativity [6, 7].

The quantum theory is defined as a linear representation of an algebra of classical observables on a Hilbert space \mathcal{H}^o . There exist now a number of constructions of the Hilbert space \mathcal{H}^o needed for defining this representation (see [8]), which have all turned out to be unitary equivalent. We will start here from the Schrödinger-like representation of \mathcal{H}^o as an L_2 space of functionals over the configuration space [36].

More precisely, as it is usually the case in quantum field theory [39], \mathcal{H}^o is defined as a space of functionals over a suitable completion $\overline{\mathcal{A}}$ of the configuration space \mathcal{A} , formed by “generalized connections”, or “distributional connections”.

2.1. State space

In order to define a generalized connection, we need some definitions. An *edge* \mathbf{e} is an oriented, 1-dimensional sub-manifold of Σ with two boundary points, called *vertices*, which is analytic everywhere, including the vertices. A generalized connection \bar{A} in $\overline{\mathcal{A}}$ is defined [13, 40] as a map that assigns an element $\bar{A}(\mathbf{e})$ of $SU(2)$ to each oriented edge \mathbf{e} in Σ , satisfying the following requirements: i) $\bar{A}(\mathbf{e}^{-1}) = (\bar{A}(\mathbf{e}))^{-1}$; and, ii) $\bar{A}(\mathbf{e}_2 \circ \mathbf{e}_1) = \bar{A}(\mathbf{e}_2) \cdot \bar{A}(\mathbf{e}_1)$. Here \mathbf{e}^{-1} is obtained from \mathbf{e} by reversing its orientation, $\mathbf{e}_2 \circ \mathbf{e}_1$ denotes the composition of the two edges (obtained by connecting the end of \mathbf{e}_1 with the beginning of \mathbf{e}_2) and $\bar{A}(\mathbf{e}_2) \cdot \bar{A}(\mathbf{e}_1)$ is the composition in $SU(2)$. Any smooth connection A is also a generalized connection: the group element that it assigns to an edge \mathbf{e} is the parallel transport along \mathbf{e} , that is $\bar{A}(\mathbf{e}) = h_{\mathbf{e}}(A) := \mathcal{P} \exp(-\int_{\mathbf{e}} A)$. Accordingly, we refer to $\bar{A}(\mathbf{e})$ as “the parallel transport of the generalized connection \bar{A} ”, in the same spirit in which we write $\delta(f) = \int dx \delta(x) f(x)$ for the Dirac δ -“function”. One can view the space $\overline{\mathcal{A}}$ of the generalized connections as the closure of the configuration space \mathcal{A} in a suitable topology.

There exist a natural measure μ^o on $\overline{\mathcal{A}}$, induced by the Haar measure on $SU(2)$, denoted the Ashtekar-Lewandowski-Baez measure. Its explicit form can be given as follows. A *graph* γ in Σ is a collection of edges such that if two distinct edges meet, they do so only at the vertices. A vertex v is called *n*-valent or of valence *n* if it has *n* adjacent edges. Fix a graph γ with *N* edges $\mathbf{e}_1, \dots, \mathbf{e}_N$, and consider the functions $\Psi_{\gamma, \psi}$ on $\overline{\mathcal{A}}$ of the form $\Psi_{\gamma, \psi}(\bar{A}) = \psi(\bar{A}(\mathbf{e}_1), \dots, \bar{A}(\mathbf{e}_N))$ for some smooth function ψ on $[SU(2)]^N$. These are cylindrical functions, since they depend only on a finite subset of the infinite “coordinates” of $\overline{\mathcal{A}}$. The measure μ^o is defined by (its cylindrical projection)

$$\int_{\overline{\mathcal{A}}} d\mu^o(\bar{A}) \Psi_{\gamma, \psi}(\bar{A}) = \int_{SU(2)^n} d^n \mu_H(g_1, \dots, g_N) \psi(g_1, \dots, g_N), \quad (2.2)$$

where μ_H is the Haar measure on $SU(2)$. We use the Hilbert space $\mathcal{H}^o := L^2(\overline{\mathcal{A}}, d\mu^o)$ of square-integrable functions on $\overline{\mathcal{A}}$ as the (kinematical) Hilbert space of the theory. (“Kinematical” in the sense of Dirac – the physical Hilbert space is then obtained by imposing the quantum constraints.) The elements of \mathcal{H}^o can be viewed as wave functions of (generalized) connections, analogous to the wave functions of distributional fields in the Schrödinger representation of a free field theory. The cylindrical functions are dense in \mathcal{H}^o ; they represent “typical” normalizable states.

Let us now discuss the $SU(2)$ gauge invariance. A generalized gauge transformation is a map g which assigns an $SU(2)$ element $g(x)$ to each point x of Σ . It acts on \bar{A} at the end points of edges: $\bar{A}(\mathbf{e}) \rightarrow g(v_+)^{-1} \cdot \bar{A}(\mathbf{e}) \cdot g(v_-)$, where v_- and v_+ are the beginning and the end point of \mathbf{e} . The space of the equivalence classes of generalized connections under generalized gauge transformations is denoted $\overline{\mathcal{A}}/\mathcal{G}$. The measure μ^o induces a natural measure $\tilde{\mu}^o$ on $\overline{\mathcal{A}}/\mathcal{G}$, obtained by the push-forward of μ^o under the projection map that sends $\overline{\mathcal{A}}$ to $\overline{\mathcal{A}}/\mathcal{G}$.

The gauge invariant functions form the $SU(2)$ gauge invariant Hilbert space $\tilde{\mathcal{H}}^o := L^2(\overline{\mathcal{A}}/\mathcal{G}, d\tilde{\mu}^o)$. These are the solutions of the $SU(2)$ constraint. Since the spaces under consideration are compact and measure-normalized, we can regard $\tilde{\mathcal{H}}^o$

as the gauge invariant sub-space of the Hilbert space $\mathcal{H}^o := L^2(\bar{\mathcal{A}}, d\mu^o)$ [13, 40, 41]. Thus, the $SU(2)$ gauge invariant quantum states can be expressed as complex-valued, square-integrable functions on $\bar{\mathcal{A}}/\mathcal{G}$, or, equivalently, as \mathcal{G} -invariant square-integrable functions on $\bar{\mathcal{A}}$.

2.2. Spin network basis

In order to work on a Hilbert space it is convenient to have a basis. A very convenient basis in \mathcal{H}^o is formed by the spin network states. These are obtained by using the fact that functions on $SU(2)$ can be expanded in irreducible representations. Given N irreducible representations j_1, \dots, j_N of $SU(2)$, we define an invariant tensor $c^{m_{k+1} \dots m_N}_{m_1 \dots m_k}$ as a multi-linear map from $\bigotimes_{I=1}^k j_I$ to $\bigotimes_{I=k+1}^N j_I$ that transforms covariantly, namely such that:

$$\begin{aligned} c^{n_{k+1} \dots n_N}_{n_1 \dots n_k} &= \\ &= j_{k+1}(g)^{n_{k+1}}_{m_{k+1}} \dots j_N(g)^{n_N}_{m_N} c^{m_{k+1} \dots m_N}_{m_1 \dots m_k} j_1(g^{-1})^{m_1}_{n_1} \dots j_N(g^{-1})^{n_k}_{m_k}, \end{aligned} \quad (2.3)$$

for arbitrary $g \in SU(2)$, where $j_I(g)$ is the matrix representing g in the representation j_I . Such an invariant tensor is also called an *intertwining tensor* from the representations j_1, \dots, j_k to j_{k+1}, \dots, j_N . All invariant tensors are given by the standard Clebsch-Gordan theory.

An *extended spin network* s is defined as a quintuple $s = (\gamma, \vec{j}, \vec{c}, \vec{\rho}, \vec{M})$ consisting of:

- A graph γ in Σ ;
- A labeling $\vec{j} := (j_1, \dots, j_N)$ of the edges $\mathbf{e}_1, \dots, \mathbf{e}_N$ of the graph γ with non-trivial irreducible representations of $SU(2)$. We refer to p_I , equal to twice the spin of the representation j_I , as the *color* of the edge \mathbf{e}_I ;
- A labeling $\vec{\rho} := (\rho_1, \dots, \rho_V)$ of the vertices v_1, \dots, v_V of γ with (possibly trivial) irreducible representations of $SU(2)$, with the constraint that for every vertex v_α the representation ρ_α sits in the tensor product of the representations assigned to the edges adjacent to v_α ;
- A labeling $\vec{c} := (c_1, \dots, c_V)$ of the vertices v_1, \dots, v_V of γ with invariant tensors; more precisely, assigned to a vertex v_α is an intertwining tensor c_α from the representations assigned to incoming edges and ρ_α to the representations assigned to the outgoing edges;
- A labeling $\vec{M} := (M_1, \dots, M_V)$ of the vertices v_1, \dots, v_V of γ which assigns a vector M_α in the representation ρ_α to every vertex v_α .

The (extended) spin network state Ψ_s is defined as follows. Consider the “parallel propagator” $\bar{A}(\mathbf{e}_I)$ of \bar{A} along each edge \mathbf{e}_I of γ , in the representation j_I . Contract these parallel propagators at each vertex v_α , using the invariant tensor c_α . Contract the leftover indices of c_α at each vertex v_α with the vector M_α assigned to the vertex. Formally:

$$\Psi_s(\bar{A}) := \left[\bigotimes_{I=1}^N j_I(\bar{A}(\mathbf{e}_I)) \otimes \bigotimes_{\alpha=1}^V M_\alpha \right] \cdot \left[\bigotimes_{\alpha=1}^V c_\alpha \right]. \quad (2.4)$$

Here ‘ \cdot ’ stands for contracting, at each vertex v_α of γ , the upper-indices of the matrices corresponding to all the incoming edges, the lower indices of the matrices assigned to all the outgoing edges and the upper index of the vector M_α with all the corresponding indices of c_α . Ψ_s is a C^∞ cylindrical function on $\bar{\mathcal{A}}$.

The introduction of the vectors M has the sole purpose of avoiding the choice of a preferred basis in the $SU(2)$ representations. If we introduce such a preferred basis, we can replace the M 's with the specification of a basis vector. In other words, the extended spin network states have a free index at each vertex v_α , living in the representation ρ_α . Below, we will find it more convenient to use the physicist-style indices, rather than the mathematician-style M notation.

For any spin network s , Ψ_s is a function on $\overline{\mathcal{A}}$ which is square-integrable with respect to the measure μ^o . We can fix a basis in the (finite dimensional) space of the invariant tensors at each vertex, and a basis in each representation ρ_α , and restrict \vec{c} and \vec{M} to basis elements. The resulting set of spin network states form a basis in \mathcal{H}^o .

It is easy to see that a spin network state Ψ_s is gauge invariant if and only if all the representations in $\vec{\rho}$ are trivial. The gauge invariant spin network states are therefore characterized solely by the graph γ , the labelings j of the edges and the intertwiners \vec{c} at the vertices. The inclusion of the representations $\vec{\rho}$ and the vectors \vec{M} at the vertices yields the extension of the spin network technology to the gauge non-invariant states, namely the extension from $\tilde{\mathcal{H}}^o$ to \mathcal{H}^o .

2.3. Loop states

An *open loop* $l = (\mathbf{e}_1, \dots, \mathbf{e}_n, M_-, M_+)$ is defined by an oriented open line in Σ formed by a sequence of edges $\mathbf{e}_1, \dots, \mathbf{e}_n$, and by two vectors (M_-, M_+) in the fundamental representation of $SU(2)$. A *loop* $\alpha = (\mathbf{e}_1, \dots, \mathbf{e}_n)$ is defined as a closed line formed by a sequence of edges. An *open loop state* is defined by $\Psi_l(\vec{A}) = M_- \cdot j(\vec{A}(\mathbf{e}_1)) \cdot \dots \cdot j(\vec{A}(\mathbf{e}_n)) \cdot M_+$. A *loop state* is defined as $\Psi_\alpha(\vec{A}) = \text{Tr}[j(\vec{A}(\mathbf{e}_1)) \cdot \dots \cdot j(\vec{A}(\mathbf{e}_n))]$, where j is the fundamental (spin 1/2) representation of $SU(2)$. Sums of products of open loop states span \mathcal{H}^o , and sums of products of loop states span $\tilde{\mathcal{H}}^o$. Products of loop states are called *multiple loop states*. Thus the multiple loop states span $\tilde{\mathcal{H}}^o$; however, they do not form a true basis, but only an overcomplete basis. This is the overcomplete basis that was used in loop quantum gravity before the introduction of the spin network true basis.

The relation between spin network states and loop states is as follows. Standard $SU(2)$ representation theory shows that the spin network states can all be obtained as linear combinations of products of open loop states. This is because all representations of $SU(2)$ can be obtained by tensoring the fundamental representation. Explicitly, these linear combinations are obtained by “symmetrizing the loops” along each edge as illustrated in [27]. Conversely, every product of fundamental representations can be decomposed in irreducible representations, and therefore multiple loop states can be expanded in the spin network basis. Thus, the decomposition of quantum states in the spin network basis is the decomposition of functions on $SU(2)$ in irreducible representations. See [9, 27] for details.

2.4. Operators

We shall not give here a complete construction of the operator algebra defined on \mathcal{H}^o , but only a few remarks on the operators that enter the Thiemann's definition of the HCO. These are the parallel transport operator and the volume operator. For each edge \mathbf{e} , the parallel transport operator $\hat{h}[\mathbf{e}]$ (with a free spin 1/2 index at each end of \mathbf{e}) represents the classical quantity $h_{\mathbf{e}}(A) := \mathcal{P} \exp(-\int_{\mathbf{e}} A)$, that is, the parallel propagator of the connection along \mathbf{e} . This operator is diagonal, and is given by

multiplication by $\bar{A}(\mathbf{e})$:

$$\left[\hat{h}[\mathbf{e}] \Psi \right] (\bar{A}) = \bar{A}(\mathbf{e}) \Psi(\bar{A}). \quad (2.5)$$

The action of this operator on the spin network basis is not immediate. We obtain it by decomposing the state $\hat{h}[\mathbf{e}] \Psi_s$ in the spin network basis, and this has to be worked out explicitly using (2.4). For instance, if \mathbf{e} and the graph γ do not intersect, then we have immediately that $\hat{h}[\mathbf{e}] \Psi_s = \Psi_{(s \cup \mathbf{e})}$, where $(s \cup \mathbf{e})$ is the spin network obtained by adding the (disconnected) edge \mathbf{e} to γ , and coloring it and its two open vertices with the spin-1/2 representation. As a second example, assume that \mathbf{e} sits entirely on the interior of one of the edges of s , say with label j . The decomposition of $\hat{h}[\mathbf{e}] \Psi_s$ in spin network states can then be obtained using the fact that the tensor product of two $SU(2)$ representations is a sum of irreducible representations. Since $\bar{A}(\mathbf{e})$ is in the 1/2 representation, we have in this case

$$\hat{h}[\mathbf{e}] \Psi_s = a_+ \Psi_{s_+} + a_- \Psi_{s_-} \quad (2.6)$$

where s_{\pm} are the spin networks obtained in the following way. Add two vertices to s , in correspondence to the end points of \mathbf{e} . Label the edge between these two vertices by $j \pm 1/2$. The representation ρ on the two new vertices is 1/2, and the intertwiner is the unique one on the three representations $j, j \pm 1, 1/2$. The free indices on the new vertices are the free indices of the operator, and, finally, the coefficients a_{\pm} are the two Clebsch-Gordan coefficients of the expansion of $j \otimes 1/2$. (See appendix C.) More complicated cases can be worked out in a similar way.

The rest of the elementary operators defined on \mathcal{H}^o contain \tilde{E}_i^a . These can be defined using the T^n loop operators technology [3], or using left-invariant vector fields on the group [35, 36]. Thiemann's HCO depends on the volume, which is a composite operator based on such elementary operators.

The volume operator has been constructed by Rovelli and Smolin in [11] using the T^n loop operators technology. This construction is based on a regularization and quantization of the classical volume. (An important clarification role was played by Loll's work [12] using a lattice regularization [42].) Later, Ashtekar and Lewandowski in [13] used the left-invariant vector fields technology to construct a “mathematically natural” operator V_{AL} . They presented it as “closely related” [13] to the construction of Rovelli and Smolin and to the classical volume. Lewandowski has clarified the relation between the two operators, showing that the difference between the two can be interpreted as due to different regularization choices – not to the technique employed (both operators can be constructed in each approach) [15]. See Appendix A. The two operators have the same action on generic trivalent vertices (tangents of adjacent edges non coplanar), which is the only case we consider here. In the following we need the explicit action of the volume operator. This has been worked out by DePietri and Rovelli in [9]. See Appendix A. Thiemann has also derived various matrix elements of the volume operator in [43] using a different technique and confirming the results of [9].

3. Graphical binor representation

In [37] it was shown that computations in the connection representation of quantum gravity can be performed using the graphical Penrose binor calculus [44] (as originally suggested by Smolin). The main ingredients of this calculus are summarized in

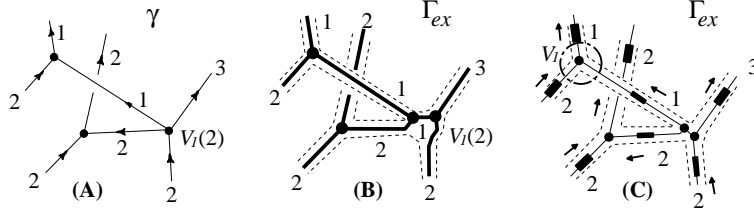


Figure 1. A spin network states and its graphical representations.

Appendix B. Furthermore, it was shown in [37] that this graphical binor calculus is fully equivalent to the loop representation developed in [3, 11, 27, 9]. These results were obtained in the gauge-invariant context, but there is no restriction to gauge invariant functions in the rules of Penrose binor calculus, therefore they extend immediately to the case of gauge non-invariant cylindrical functions. Let us review these results.

Following [37], we associate a graphical representation *a la* Penrose to each cylindrical function $\Psi_{\gamma, \psi}^\dagger$. As a first step, we consider a projection of the graph γ on a plane and construct its extended planar graph Γ_{ex} (see figure 1(B) and [9]). The extended planar graph is a two dimensional “thickening out” the graph: an oriented two-dimensional surface with the topology of $\gamma \times [0, 1]$. Next, we expand the cylindrical function as a sum of products of irreducible representation on the edges. For each term of the sum, we insert the Penrose graphical representation of the matrices $j_I(\bar{A}(\mathbf{e}_I))$ in the corresponding edges \mathbf{e}_I of the extended planar graph, using equation (B.6). Next, we insert the graphical representation of the contractions c_α in each vertex v_α , using equations (B.7) and (B.8). Finally, lines corresponding to summed dummy indices are connected, with an additional factor $(-1)^p$ for each trace (closing a loop); here p is the color of the representation in which the index lives (see (B.3)). It follows from equation (B.9) that the planar graphical representation is independent from the orientation of the edges. Finally, we notice that the Penrose convention of indicating tensors by means of filled boxes is superfluous in this context, because a colored line that runs along an edge of the extended graphs always carries a parallel propagator. Thus the information given by the boxes is already contained in the fact that the line runs along an edge, and we can drop the boxes.

In particular, we obtain in this manner a graphical representation for each spin-network state. Let us focus on these. First of all, in a spin network state we have a single irreducible tensor on each edge. Therefore each edge carries a single colored line (recall: color is twice spin). Second, at each vertex v_α we have an intertwining tensor c_α . The graphical representation of each invariant tensor can be given by means of a trivalent tree-like graph (with open ends connected to the lines in the adjacent edges). This is a consequence of equation (B.8). We denote the “internal” edges of this trivalent decomposition as “virtual edges”. It is important to keep in mind that virtual edges are drawn with finite length on the extended planar graph, but they do not represent finitely extended objects on the space manifold Σ – they are simply a graphical representation of the index pattern of combinations of the $SU(2)$ indices of Clebsch-Gordan coefficients. They characterize an intertwiner by giving its expansion in Clebsch-Gordan coefficients. Finally, at each vertex we have a representation ρ_α ,

[†] More precisely we define the graphical binor representation of polynomial cylindrical functions, i.e., functions that are polynomial in the $SU(2)$ matrices $\mathbf{g}_\mathbf{e} = h_\mathbf{e}(\bar{A})$ associated to each edge \mathbf{e} of γ .

and a vector M_α (or a free index) sitting in this representation, contracted with the invariant tensor. Accordingly, in the graphical representation of the spin network state we have one of the virtual edges which is not attached to any external line. This free end is missing if ρ_α is the trivial representation, namely if the vertex is gauge invariant.

In figure 1 we show, as an example, **(A)**: a spin network (in the connection representation) determined by an oriented graph, and the labels of edges and vertices. **(B)** A spin-network in the loop representation and its extended planar graph (as in [9]). **(C)** The planar binor representation on the extended planar graph of the cylindrical function given by the spin-network.

A simple advantage of this graphical representation is due to the fact that planar graphs are easier to manipulate than expressions with a large number of indices. But the main advantage is due to the peculiar nature of the tensors involved, which are based on $SU(2)$ matrices. These tensors satisfy some basic relations that are translated into simple graphical formulas. The prototype of these is equation (B.4), from which (as shown by Kauffman and Lins [31]) all the other graphical relations can be derived. These graphical relations are the reason for the great utility of graphical recoupling theory, well known and much exploited in nuclear, atomic and molecular physics (where $SO(3)$ plays a major role). The important formulas satisfied by the graphical representations of the quantum states are summarized in Appendix C. The calculations in this paper rely heavily on these formulas.

As an example, consider the action of the holonomy operator $\hat{h}[\mathbf{e}_I]$ on a spin network state Ψ_s , given in (2.5). Consider the particular case in which \mathbf{e} sits on the interior of an edge \mathbf{e}' of s . Following the prescription given above, the graphical representation of the r.h.s. of (2.5) is simply obtained by adding a line colored 1, inside the (expanded) edge \mathbf{e}' . The expansion of this state in spin network states is then immediately given graphically by (C.10).

Notice that, following [37], we have fully recovered in this way the “pure” loop representation of quantum gravity, in which states and operators can be defined without any reference to the Schrödinger-like functions of connections. In the same fashion, the Dirac energy-basis $|n\rangle$ representation of the harmonic oscillator allows us to formulate and solve the theory without reference to its Schrödinger representation. However, here we have recovered the loop representation starting from the gauge non-invariant connection representation. Thus we have obtained the generalization of the loop representation to gauge non-invariant states. This generalization is simply contained in the fact that the spin networks can have (colored) open ends at the vertices. Of course, one might have avoided the detour through the connection representation, and might have directly defined the loop representation as a suitable representation of an appropriate algebra of gauge non-invariant observables. This can be done, but we have preferred here the long way, in order to make the link with the connection representation (using which Thiemann constructed the HCO) fully explicit.

4. Thiemann’s Hamiltonian constraint operator.

The Hamiltonian constraint of general relativity can be written as

$$\mathcal{H} = \frac{1}{\sqrt{\det(q)}} \text{Tr}((F_{ab} - 2[K_a, K_b])[E^a, E^b])$$

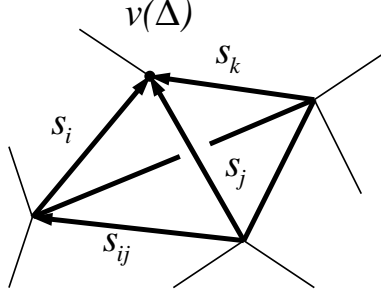


Figure 2. An elementary tetrahedron and the orientation choice of the edges.

$$= \mathcal{H}^E - \frac{2}{\sqrt{\det(q)}} \text{Tr}[K_a, K_b][E^a, E^b]. \quad (4.1)$$

F_{ab} is the curvature of A_a^i , and K_a is related to the extrinsic curvature of the spatial manifold Σ . This is the form that the constraint of the Lorentzian theory takes when written in terms of the real connection. Both (A_a^i, \tilde{E}_i^a) and (\tilde{E}_i^a, K_a^i) are canonical pairs of variables. K_a^i is related to A_a^i by $A_a^i = \Gamma_a^i - \text{sgn}(e)K_a^i$, where Γ_a^i is the spin-connection annihilating the triad and $\text{sgn}(e)$ is the sign of the determinant of undensitized triad e_a^i . There are two important differences between this connection and the one introduced by Ashtekar. First, all variables are real, while the Ashtekar connection, $A_a^i = \Gamma_a^i + i \text{sgn}(e)K_a^i$, is complex. Second, the constraint (4.1) contains the factor of one over the square root of the metric. In Ashtekar's theory this factor is absorbed into the lapse function. The first term in the right hand side of (4.1) defines the hamiltonian constraint for gravity with euclidean signature – accordingly, \mathcal{H}^E is called the euclidean hamiltonian constraint.

In order to simplify the hamiltonian constraint, Thiemann [22] uses the following identities

$$\frac{[E^a, E^b]^i}{\sqrt{\det q}} = \frac{2}{G} \epsilon^{abc} \{A_c^i, V\} \quad (4.2)$$

and

$$K_a^i = \frac{1}{G} \{A_c^i, K\}, \quad (4.3)$$

where V is the volume of Σ :

$$V = \int_{\Sigma} d^3x \sqrt{\det q} = \int_{\Sigma} d^3x \sqrt{\left| \frac{1}{3!} \epsilon_{abc} \epsilon^{ijk} \tilde{E}_i^a \tilde{E}_j^b \tilde{E}_k^c \right|}, \quad (4.4)$$

and K is the integrated trace of the densitized extrinsic curvature of Σ :

$$K = \int_{\Sigma} d^3x K_a^i \tilde{E}_i^a. \quad (4.5)$$

Using the identities (4.2) and (4.3) we can write the euclidean hamiltonian constraint as:

$$\mathcal{H}^E[N] = \frac{2}{G} \int_{\Sigma} d^3x N(x) \epsilon^{abc} \text{Tr}(F_{ab}\{A_c, V\}), \quad (4.6)$$

and the total hamiltonian constraint (4.1) then takes the form:

$$\mathcal{H}[N] = \mathcal{H}^E[N] - \frac{8}{G^3} \int_{\Sigma} d^3x N(x) \epsilon^{abc} \text{Tr}(\{A_a, K\} \{A_b, K\} \{A_c, V\}). \quad (4.7)$$

Another useful identity expresses the extrinsic curvature (4.5) in the form:

$$K = \frac{1}{G} \{V, \mathcal{H}^E[1]\}, \quad (4.8)$$

where $\mathcal{H}^E[1]$ is the euclidean hamiltonian constraint from (4.6) for lapse function set to one.

By plugging (4.6) into (4.8) and then the result into (4.7) we have an expression for the lorentzian hamiltonian constraint defined entirely in terms of the volume and the connection. It is then relatively simple to turn this expression into an operator. In the connection representation, the connection A_a^i and the curvature F_{ab}^k act (essentially) multiplicatively. The differential part of the HCO, originating from the action of the triads, is captured by the volume operator. But the volume operator has a well understood action on the kinematical state space.

From now on, we concentrate on the euclidean term of the constraint. In the quantum theory we do not have an operator corresponding to the connection, but only an operator corresponding to its parallel transport. Accordingly, we regulate \mathcal{H}^E , expressing it in terms of parallel transports. We introduce a triangulation \mathcal{T} of Σ formed by elementary tetrahedra Δ with analytic edges. We denote by $s_i^v(\Delta)$, or simply by $s_i, i = 1, 2, 3$ the three edges meeting at a vertex $v(\Delta)$ of a tetrahedron Δ . Also $\alpha_{ij}(\Delta) := s_i(\Delta) \circ s_{ij}(\Delta) \circ s_j^{-1}(\Delta)$ is the loop, based at $v(\Delta)$ and composed out of the edges s_i, s_j^{-1} , and the corresponding edge s_{ij} of the tetrahedron (see figure 2). To start with we write the Hamiltonian constraint as a sum over all tetrahedra in the triangulation

$$\mathcal{H}^E[N] = \sum_{\Delta \in \mathcal{T}} \mathcal{H}_{\Delta}^E[N] = \sum_{\Delta \in \mathcal{T}} \int_{\Delta} d^3x N(x) \epsilon^{abc} \text{Tr}(F_{ab} \{A_c, V\}). \quad (4.9)$$

In the limit in which a tetrahedron Δ shrinks to a point $v(\Delta)$ the Hamiltonian constraint over Δ is

$$\mathcal{H}_{\Delta}^E[N] = \left(-\frac{2}{3G}\right) N(v(\Delta)) \epsilon^{ijk} \text{Tr}(h_{\alpha_{ij}} h_{s_k} \{h_{s_k}^{-1}, V\}) + \mathcal{O}(V(\Delta)^{4/3}) \quad (4.10)$$

where $V(\Delta)$ is the volume of the tetrahedron Δ . In the above expression $h_{\alpha_{ij}}$ is the holonomy along the closed loop α_{ij} and h_{s_k} is the holonomy along the open loop segment s_k . That the above limit gives the correct expression (4.9) follows from the expansions:

$$\lim_{\Delta \rightarrow v(\Delta)} h_{\alpha_{ij}} = 1 + \frac{1}{2} F_{ab} s_i^a s_j^b \quad (4.11)$$

and

$$\lim_{\Delta \rightarrow v(\Delta)} h_{s_k} = 1 + A_c s_k^c. \quad (4.12)$$

Thus, if we have a sequence $n \mapsto \mathcal{T}_n$ of finer and finer triangulations of Σ , we can write

$$\mathcal{H}^E[N] = \lim_{n \rightarrow \infty} \sum_{\Delta \in \mathcal{T}_n} \mathcal{H}_{\Delta}^E[N]. \quad (4.13)$$

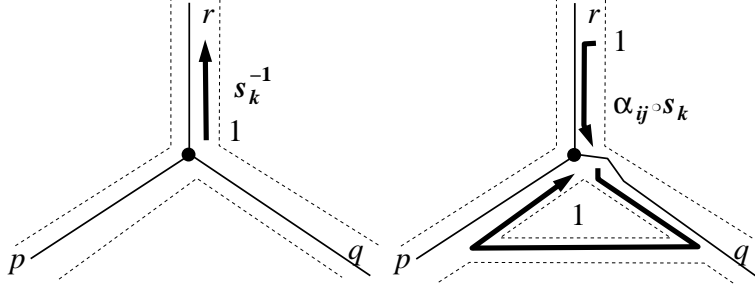


Figure 3. The “small open loops” of the Hamiltonian operator. Notice that in gauge non-invariant states (states with open ends in the graphical representation) orientation matter. Two open ends can be joined only if their orientation is consistent.

Since the operators corresponding to the classical quantities h and V are well understood, this equation provides an expression for the constraint which is appropriate for quantization. However, by simply turning this expression into an operator, with an arbitrary chosen sequence of triangulations, one obtains meaningless results. Following Thiemann, we define the quantum Hamiltonian operator by adapting the regularization to the state. For every state $\Psi_{\gamma,\psi}$, we define

$$\hat{\mathcal{H}}^E[N] \Psi_{\gamma,\psi} = \lim_{n \rightarrow \infty} \sum_{\Delta \in \mathcal{T}_n^{(\gamma)}} \hat{\mathcal{H}}_\Delta^E[N] \Psi_{\gamma,\psi} \quad (4.14)$$

where

$$\begin{aligned} \hat{\mathcal{H}}_\Delta^E[N] &= N(v(\Delta)) \hat{\mathcal{H}}_\Delta^E = N_v \hat{\mathcal{H}}_\Delta^E \\ \hat{\mathcal{H}}_\Delta^E &= -\frac{2}{3il_0^2} \epsilon^{ijk} \text{Tr} \left(\frac{\hat{h}_{\alpha ij} - \hat{h}_{\alpha ji}}{2} \hat{h}_{s_k} [\hat{h}_{s_k}^{-1}, V] \right), \end{aligned} \quad (4.15)$$

and $\mathcal{T}_n^{(\gamma)}$ is a sequence of triangulations satisfying the following condition: (for each n) there is a vertex $v(\Delta)$ sitting on each of the vertices v of γ ; and if the vertex v is k -valent then the corresponding vertex $v(\Delta)$ has precisely k adjacent edges, each contained in one of the k edges of γ adjacent to v . The triangulation is arbitrary elsewhere. Since the classical expression converges to the correct hamiltonian constraint for any sequence of triangulations, this choice does not spoil the formal classical limit of the operator. On the other hand, this choice yields a well defined, diffeomorphism-covariant and non-trivial operator. This completes the definition of the quantum operator.

Simple manipulations then show that the action of this operator can be written as

$$\hat{\mathcal{H}}_\gamma^E[N] \Psi_{\gamma,\psi} = \sum_{v \in \mathcal{V}(\gamma)} 8N_v \sum_{v(\Delta)=v} \hat{H}_\Delta^E \frac{p_\Delta}{E(v)} \Psi_{\gamma,\psi}, \quad (4.16)$$

where $\mathcal{V}(s)$ is the set of the vertices of s ; \hat{H}_Δ^E is defined by (4.15); p_Δ is one, whenever Δ is a tetrahedron with three edges coinciding with three edges of the spin network state joined at the vertex v , and zero otherwise. $E(v)$ is the number of non-coplanar triples of edges of γ at the vertex v . In the case of an n -valent vertex having no triples of coplanar edges $E(v) = n(n-1)(n-2)/6$. Also N_v is the value of the lapse function at the vertex (see [22] for details).

Clearly $\hat{\mathcal{H}}_\Delta^E$ of (4.15) it is not the only operator that has (4.10) for classical limit. Any other ordering of the operators $\hat{h}_{\alpha_{ij}}$, \hat{h}_{s_k} and $[\hat{h}_{s_k}^{-1}, V]$ gives (4.10). We will consider the action of Thiemann's Hamiltonian constraint with the two orderings

$$\hat{\mathcal{H}}_\Delta^{E(1)} = -\frac{2}{3il_0^2}\epsilon^{ijk}\text{Tr}\left(\frac{\hat{h}_{\alpha_{ij}} - \hat{h}_{\alpha_{ji}}}{2}\hat{h}_{s_k}[\hat{h}_{s_k}^{-1}, V]\right) \quad (4.17)$$

$$\hat{\mathcal{H}}_\Delta^{E(2)} = -\frac{2}{3il_0^2}\epsilon^{ijk}\text{Tr}\left(\hat{h}_{s_k}[\hat{h}_{s_k}^{-1}, V]\frac{\hat{h}_{\alpha_{ij}} - \hat{h}_{\alpha_{ji}}}{2}\right) \quad (4.18)$$

which correspond to the cases analyzed by Thiemann [22].

To compute the action of (4.17) and (4.18) on trivalent vertices, it is sufficient to compute

$$\hat{\mathcal{H}}_\Delta^{E(1)} \Psi_{\gamma,\psi} = \frac{2i}{3l_0^2}\epsilon^{ijk}\text{Tr}\left[\frac{\hat{h}_{\alpha_{ij}} - \hat{h}_{\alpha_{ji}}}{2}\hat{h}_{s_k}\hat{V}\hat{h}_{s_k}^{-1}\right] \Psi_{\gamma,\psi}, \quad (4.19)$$

$$\hat{\mathcal{H}}_\Delta^{E(2)} \Psi_{\gamma,\psi} = \frac{2i}{3l_0^2}\epsilon^{ijk}\text{Tr}\left[\hat{h}_{s_k}\hat{V}\hat{h}_{s_k}^{-1}\frac{\hat{h}_{\alpha_{ij}} - \hat{h}_{\alpha_{ji}}}{2}\right] \Psi_{\gamma,\psi}; \quad (4.20)$$

because the volume annihilates the gauge-invariant trivalent vertices and therefore the other term of the commutators vanishes. In section 5.3, we show that these two choices exhaust all possible “natural” orderings.

5. Calculation of the HCO matrix elements

The action of the HCO is local, namely it is a sum of independent actions on each vertex. Therefore we can focus on its action on a single vertex v . Let us consider the action of the operator $\hat{\mathcal{H}}_\Delta^E$ on a single trivalent vertex with edges $\mathbf{e}_i, \mathbf{e}_j, \mathbf{e}_k$ with colors p, q, r . We indicate the part of the spin network state, containing only the vertex v and its adjacent edges as $|v\rangle$.

5.1. First ordering choice

We investigate the action of the Euclidean Hamiltonian operator $\hat{\mathcal{H}}_\Delta^{E(1)}$ on $|v\rangle$

$$\hat{\mathcal{H}}_\Delta^{E(1)} |v\rangle = -\frac{2i}{3l_0^2}\epsilon^{ijk}\frac{\hat{h}[\alpha_{ij}] - \hat{h}[\alpha_{ji}]}{2}\hat{h}[s_k]\hat{V}\hat{h}[s_k^{-1}] |v\rangle \quad (5.1)$$

As described in sections 2 and 3, $\hat{h}[s_k^{-1}]$ attaches an open loop segment s_k^{-1} to the edge \mathbf{e}_k with color r . It creates one additional vertex on \mathbf{e}_k , and alters the color of the edge segment between the two vertices of s_k . From (C.10) we have

$$\hat{h}[s_k^{-1}] \begin{array}{c} \text{---} \mathbf{r} \text{---} \\ | \\ \text{---} \mathbf{p} \text{---} \mathbf{q} \end{array} = \sum_{\epsilon=\pm 1} a_\epsilon(r) \begin{array}{c} \text{---} \mathbf{r} \text{---} \mathbf{1} \text{---} \\ | \\ \text{---} \mathbf{p} \text{---} \mathbf{q} \end{array} \quad (5.2)$$

From Appendix C, the coefficients $a_\pm(r)$ are

$$a_+(r) = 1, \quad a_-(r) = -\frac{r}{r+1}. \quad (5.3)$$

Notice that the (lower) open end in the right hand side of (5.2) is located at the vertex. Thus, the vertex has now become gauge non-invariant: it carries the spin-1/2 representation, with a free index, and its interwiner is determined by the the virtual edge of color r .

The volume operator acts on this vertex. The action of the volume operator has been computed for gauge invariant states only, but a moment of reflection shows that the results in the gauge invariant case are relevant for the present case as well. In fact (in both its definitions) the volume operator acts on the (real!) edges adjacent to the vertex, giving a sum of terms – one term per triple of edges. If we act on a gauge-invariant 4-valent vertex, we obtain a sum of four terms, one for each triple of edges. In the present case, the volume acts on the three real edges, giving a single term, but the action of this single term is precisely equivalent to the action of one of the four terms of the volume over a four-valent gauge invariant vertex (See Appendix A). The free index of the vertex behaves as the fourth edge, but it is “invisible” for the operator. Therefore the action of \hat{V} can be immediately obtained from the expression of \hat{V} on 4-valent gauge-invariant vertices, which was given in [9], and is recalled in Appendix A. In particular, we show in Appendix A that for the combination of colors in (5.2) this action is diagonal. Using (A.11), we obtain

$$\hat{V}\hat{h}[s_k^{-1}] = \frac{l_0^3}{4} \sum_{\epsilon=\pm 1} a_\epsilon(r) \sqrt{w(p, q, r + \epsilon, 1)} \quad (5.4)$$

where $w(, , ,)$ is given in (A.10).

The next step is to compute the action of $\hat{h}[\alpha_{ij}]\hat{h}[s_k]$ on the right hand side of (5.4). This operator attaches α_{ij} and s_k to the open ends in (5.4) according to the prescription given by the orientation of the open loops. Finally, the trace connects the free indices. This is represented in the graphical computation by tying up the open ends of the virtual edges (see figure 4). Moreover, we have to add a minus sign due to the trace prescription of the graphical representation (see section 3). We obtain

$$\left[\frac{\hat{h}[\alpha_{ij}]\hat{h}[s_k] - \hat{h}[\alpha_{ji}]\hat{h}[s_k]}{2} \right] \quad (5.4) \quad =$$

$$= (-1) \frac{1}{2} \left[\text{Diagram 1} - \text{Diagram 2} \right] =$$

$$= (-1) \sum_{\bar{\epsilon}=\pm 1} \sum_{\tilde{\epsilon}=\pm 1} a_{\bar{\epsilon}}(p) a_{\tilde{\epsilon}}(q) \cdot \text{Diagram} \quad (5.5)$$

In the last equation we used the fact that the anti-symmetrization of two loops is equivalent to two 3-vertices of type (1,1,2) and we applied equation (C.10) to the p and q edges. Now, the tangle around the vertex in the right hand side of (5.5) can be evaluated using recoupling theory. We have (see Appendix C)

$$\text{Diagram} = \frac{\text{Diagram}_1}{\text{Diagram}_2} \cdot \text{Diagram}_3 \quad (5.6)$$

In (5.6) we have not shown the bottom link of (5.5). Using equations (C.11) end (C.9) we expand the right hand side of (5.6)

$$\begin{aligned} \text{Diagram} &= \left[\frac{p}{r} \text{Diagram}_1 - \frac{q}{r} \text{Diagram}_2 \right] = \\ &= \left[\frac{p}{r} \frac{\text{Diagram}_3}{\text{Diagram}_4} - \frac{q}{r} \frac{\text{Diagram}_5}{\text{Diagram}_6} \right] \cdot \text{Diagram}_7 \end{aligned} \quad (5.7)$$

The chromatic evaluation of the closed nets in equations (5.6) and (5.7) gives

$$R_1(r, \epsilon) = a_\epsilon(r) \cdot \frac{\text{Diagram}_1}{\text{Diagram}_2} = \epsilon \frac{r}{r+1} \quad (5.8)$$

$$R_2(p, \bar{\epsilon}; q, \tilde{\epsilon}; r) = a_{\bar{\epsilon}}(p) a_{\tilde{\epsilon}}(q) \left[\frac{p}{r} \frac{\text{Diagram}_3}{\text{Diagram}_4} - \frac{q}{r} \frac{\text{Diagram}_5}{\text{Diagram}_6} \right] \cdot \frac{\text{Diagram}_7}{\text{Diagram}_8} \quad (5.9)$$

$$= \begin{cases} \frac{p-q}{2r} & ; \quad \bar{\epsilon} = +1, \tilde{\epsilon} = +1 \\ -\frac{(q-p+r)(2+p+q)}{4r(1+q)} & ; \quad \bar{\epsilon} = -1, \tilde{\epsilon} = +1 \\ \frac{4r(1+q)}{(p-q+r)(2+p+q)} & ; \quad \bar{\epsilon} = +1, \tilde{\epsilon} = -1 \\ \frac{4r(1+p)}{(p-q)(p+q-r)(2+p+q+r)} & ; \quad \bar{\epsilon} = -1, \tilde{\epsilon} = -1 \end{cases}$$

We have obtained

$$\text{Tr} \left(\frac{\hat{h}_{\alpha_{ij}} - \hat{h}_{\alpha_{ji}}}{2} \hat{h}_{s_k} \hat{V} \hat{h}_{s_k}^{-1} \right) \text{ (diagram)} = -l_0^3 \sum_{\bar{\epsilon}, \tilde{\epsilon} = \pm 1} A^{(0)}(p, \bar{\epsilon}; q, \tilde{\epsilon}; r) \text{ (diagram)} .$$

where

$$A^{(0)}(p, \bar{\epsilon}; q, \tilde{\epsilon}; r) = \sum_{\epsilon = \pm 1} \frac{1}{4} \sqrt{w(p, q, r + \epsilon, 1)} R_1(r, \epsilon) R_2(p, \bar{\epsilon}; q, \tilde{\epsilon}, r). \quad (5.10)$$

Collecting our results we obtain that the action of Thiemann's Euclidean HCO on a generic 3-vertex $|v(p, q, r)\rangle$ is given by:

$$\begin{aligned} \hat{\mathcal{H}}_{\Delta}^{E(0)} |v(p, q, r)\rangle &= \frac{2il_0}{3} \sum_{\bar{\epsilon} = \pm 1} \sum_{\tilde{\epsilon} = \pm 1} \left[A^{(0)}(p, \bar{\epsilon}; q, \tilde{\epsilon}; r) \left| \text{diagram} \right\rangle + \right. \\ &\quad \left. + A^{(0)}(q, \bar{\epsilon}; r, \tilde{\epsilon}; p) \left| \text{diagram} \right\rangle + A^{(0)}(r, \bar{\epsilon}; p, \tilde{\epsilon}; q) \left| \text{diagram} \right\rangle \right] \end{aligned} \quad (5.11)$$

where the coefficients A^1 are given by (5.10).

5.2. Second ordering choice

In the case of the ordering choice given by (4.20) we have to perform the computations in the reverse order. First we compute the action of the elementary loop operator $\hat{h}_{s_k}^{-1} [\hat{h}_{\alpha_{ij}} - \hat{h}_{\alpha_{ji}}]$ on $|v\rangle$, and then, the action of $\hat{h}_{s_k} \hat{V}$. Using the same technique as in the previous section we get:

$$\hat{h}_{s_k}^{-1} \frac{\hat{h}_{\alpha_{ij}} - \hat{h}_{\alpha_{ji}}}{2} \text{ (diagram)} = \text{diagram} = \text{diagram} \quad (5.12)$$

$$\begin{aligned}
&= \sum_{\epsilon=\pm 1} \sum_{\bar{\epsilon}=\pm 1} \sum_{\tilde{\epsilon}=\pm 1} a_{\epsilon}(r) a_{\bar{\epsilon}}(p) a_{\tilde{\epsilon}}(q) \quad \text{Diagram 1} = \\
&= \sum_{\epsilon, \bar{\epsilon}, \tilde{\epsilon}=\pm 1} \sum_{J=r, r+2\epsilon} a_{\epsilon}(r) a_{\bar{\epsilon}}(p) a_{\tilde{\epsilon}}(q) \begin{Bmatrix} r & r+\epsilon & J \\ 1 & 2 & 1 \end{Bmatrix} \quad \text{Diagram 2} = \\
&= \sum_{\epsilon, \bar{\epsilon}, \tilde{\epsilon}=\pm 1} \sum_{J=r, r+2\epsilon} a_{\epsilon}(r) \begin{Bmatrix} r & r+\epsilon & J \\ 1 & 2 & 1 \end{Bmatrix} \tilde{R}_2(p, \bar{\epsilon}; q, \tilde{\epsilon}; r, J) \quad \text{Diagram 3} .
\end{aligned}$$

We first inserted the loop corresponding to the $\hat{h}[\dots]$ operator in the extended planar graph corresponding to the 3-vertex. Then we decomposed the result, using equation (C.10). Then we have applied the recoupling theorem (C.6) to the 4-vertex $(r, r+\epsilon, 1, 2)$. Finally we have reduced the 3-vertex $(p+\bar{\epsilon}, q+\tilde{\epsilon}, J)$ to its fundamental form as in (5.5). In the last step we have defined:

$$\begin{aligned}
&\text{Diagram 4} = \frac{\tilde{R}_2(p, \bar{\epsilon}; q, \tilde{\epsilon}; r, J)}{a_{\bar{\epsilon}}(p) a_{\tilde{\epsilon}}(q)} \cdot \text{Diagram 5} \quad (5.13)
\end{aligned}$$

A direct comparison with equation (5.5) shows that for $J = r$

$$\tilde{R}_2(p, \bar{\epsilon}; q, \tilde{\epsilon}; r, r) = R_2(p, \bar{\epsilon}; q, \tilde{\epsilon}; r).$$

Computing the action of the volume and closing the trace with the \hat{h}_{s_k} operator we obtain

$$\begin{aligned}
&\text{Tr} \left(\hat{h}_{s_k} \hat{V} \hat{h}_{s_k}^{-1} \frac{\hat{h}_{\alpha_{ij}} - \hat{h}_{\alpha_{ji}}}{2} \right) \quad \text{Diagram 6} \\
&= -\frac{l_0^3}{4} \sum_{\epsilon, \bar{\epsilon}, \tilde{\epsilon}=\pm 1} \sum_{J=r, r+2\epsilon} a_{\epsilon}(r) \tilde{R}_2(p, \bar{\epsilon}; q, \tilde{\epsilon}; r, J) \times
\end{aligned}$$

$$\begin{aligned}
& \times \frac{\text{Diagram 1}}{\text{Diagram 2}} \sqrt{w(p + \bar{\epsilon}, q + \tilde{\epsilon}, r + \epsilon, 1)} \times \\
& \times \delta_J^r \frac{\text{Diagram 3}}{\text{Diagram 4}} \text{Diagram 5}
\end{aligned}$$

Diagram 1: A square with vertices labeled 1, 2, 1, 2. The top edge is labeled $r + \epsilon$, the bottom edge is labeled r , and the left edge is labeled J . The right edge is labeled J .

Diagram 2: Two circles. The left circle has a horizontal line through its center, with r above and 2 below. The right circle has a horizontal line through its center, with 1 above and $r + \epsilon$ below.

Diagram 3: A circle with a horizontal line through its center, with 1 above and $r + \epsilon$ below.

Diagram 4: A circle with a horizontal line through its center, with r above and 1 below.

Diagram 5: A vertex with three edges. The top edge is labeled r . The bottom-left edge is labeled $p + \bar{\epsilon}$. The bottom-right edge is labeled $q + \tilde{\epsilon}$. The vertex is labeled 1 .

We define

$$\begin{aligned}
A^{(2)}(p, \bar{\epsilon}; q, \tilde{\epsilon}; r) &= \sum_{\epsilon = \pm 1} \frac{1}{4} \sqrt{w(p + \bar{\epsilon}, q + \tilde{\epsilon}, r + \epsilon, 1)} \tilde{R}_2(p, \bar{\epsilon}; q, \tilde{\epsilon}; r, r) \times \\
& \times a_\epsilon(r) \frac{\text{Diagram 1}}{\text{Diagram 2}} \frac{\text{Diagram 3}}{\text{Diagram 4}} = \\
& = \sum_{\epsilon = \pm 1} \frac{1}{4} \sqrt{w(p + \bar{\epsilon}, q + \tilde{\epsilon}, r + \epsilon, 1)} R_1(r, \epsilon) R_2(p, \bar{\epsilon}; q, \tilde{\epsilon}, r).
\end{aligned} \tag{5.14}$$

Diagram 1: A square with vertices labeled 1, 1, 2, 2. The top edge is labeled $r + \epsilon$, the bottom edge is labeled r , and the left edge is labeled r . The right edge is labeled r .

Diagram 2: Two circles. The left circle has a horizontal line through its center, with r above and 2 below. The right circle has a horizontal line through its center, with 1 above and $r + \epsilon$ below.

Diagram 3: A circle with a horizontal line through its center, with 1 above and $r + \epsilon$ below.

Diagram 4: A circle with a horizontal line through its center, with r above and 1 below.

We have finally obtained the action of $\hat{\mathcal{H}}_\Delta^{E(2)}$ on non planar 3-vertices:

$$\begin{aligned}
\hat{\mathcal{H}}_\Delta^{E(2)} |v(p, q, r)\rangle &= \frac{2il_0}{3} \sum_{\bar{\epsilon} = \pm 1} \sum_{\tilde{\epsilon} = \pm 1} \left[A^{(2)}(p, \bar{\epsilon}; q, \tilde{\epsilon}; r) \left| \text{Diagram 1} \right\rangle + \right. \\
& \left. + A^{(2)}(q, \bar{\epsilon}; r, \tilde{\epsilon}; p) \left| \text{Diagram 2} \right\rangle + A^{(2)}(r, \bar{\epsilon}; p, \tilde{\epsilon}; q) \left| \text{Diagram 3} \right\rangle \right].
\end{aligned} \tag{5.15}$$

Diagram 1: A vertex with three edges. The top edge is labeled r . The bottom-left edge is labeled $p + \bar{\epsilon}$. The bottom-right edge is labeled $q + \tilde{\epsilon}$. The vertex is labeled 1 .

Diagram 2: A vertex with three edges. The top edge is labeled r . The bottom-left edge is labeled $p + \bar{\epsilon}$. The bottom-right edge is labeled $q + \tilde{\epsilon}$. The vertex is labeled 1 .

Diagram 3: A vertex with three edges. The top edge is labeled r . The bottom-left edge is labeled $p + \bar{\epsilon}$. The bottom-right edge is labeled $q + \tilde{\epsilon}$. The vertex is labeled 1 .

where the coefficients A^2 are given by (5.14). Notice that this is identical to the action of equation (5.11) with $A^{(0)}(p, \bar{\epsilon}; q, \tilde{\epsilon}; r)$ replaced by $A^{(2)}(p, \bar{\epsilon}; q, \tilde{\epsilon}; r)$.

5.3. Other orderings

Consider all the permutations of the four operator \hat{V} , \hat{h}_{s_k} , $\hat{h}_{s_k}^{-1}$ and $(\hat{h}_{\alpha_{ij}} - \hat{h}_{\alpha_{ji}})/2$. These are the “natural” orderings of the hamiltonian operator. Equations (4.19) and (4.20) exhaust the orderings in which the volume (the only operator that “grasps”

Table 1. Matrix elements $A^{(1)}(p, \bar{\epsilon}; q, \bar{\epsilon}; r)$ and $A^{(2)}(p, \bar{\epsilon}; q, \bar{\epsilon}; r)$ of the non-symmetric and symmetric euclidean Thiemann's hamiltonian constraints, for the simplest 3-vertices. We have denoted by $(p' = p \pm \bar{\epsilon}, q' = q \pm \bar{\epsilon}, r)$ the new colors of the 3-vertex.

p	q	r	$\bar{\epsilon}$	$\bar{\epsilon}$	(p', q', r)	$A^{(1)}(p, \bar{\epsilon}; q, \bar{\epsilon}; r)$	$A^{(2)}(p, \bar{\epsilon}; q, \bar{\epsilon}; r)$
1	0	1	1	1	(2,1,1)	0	$1/16 \sqrt[4]{2}$
			1	-1	(NO)	0	0
			-1	1	(0,1,1)	0	0
			-1	-1	(NO)	0	0
1	1	0	1	1	(2,2,0)	0	0
			1	-1	(NO)	0	0
			-1	1	(NO)	0	0
			-1	-1	(0,0,0)	0	0
2	0	2	1	1	(3,1,2)	0	$1/24 \sqrt[4]{60}$
			1	-1	(NO)	0	0
			-1	1	(1,1,2)	0	$-1/18 \sqrt[4]{12}$
			-1	-1	(NO)	0	0
2	2	0	1	1	(3,3,0)	0	0
			1	-1	(3,1,0)	0	0
			-1	1	(1,3,0)	0	0
			-1	-1	(1,1,0)	0	0
2	1	1	1	1	(3,2,1)	$1/16 \sqrt[4]{2}$	$1/16 \sqrt[4]{5}$
			1	-1	(3,0,1)	0	0
			-1	1	(1,2,1)	$5/48 \sqrt[4]{2}$	$5/48 \sqrt[4]{2}$
			-1	-1	(1,0,1)	$1/32 \sqrt[4]{2}$	0
1	2	1	1	1	(2,3,1)	$-1/16 \sqrt[4]{2}$	$-1/16 \sqrt[4]{5}$
			1	-1	(2,1,1)	$-5/48 \sqrt[4]{2}$	$-5/48 \sqrt[4]{2}$
			-1	1	(0,3,1)	0	0
			-1	-1	(0,1,1)	$-1/32 \sqrt[4]{2}$	0
1	1	2	1	1	(2,2,2)	0	0
			1	-1	(2,0,2)	$1/24 \sqrt[4]{12}$	0
			-1	1	(0,2,2)	$-1/24 \sqrt[4]{12}$	0
			-1	-1	(0,0,2)	0	0
2	2	2	1	1	(3,3,2)	0	0
			1	-1	(3,1,2)	$-1/12(\sqrt[4]{5} - \sqrt[4]{2})$	$-1/24 \sqrt[4]{30}$
			-1	1	(1,3,2)	$1/12(\sqrt[4]{5} - \sqrt[4]{2})$	$1/24 \sqrt[4]{30}$
			-1	-1	(1,1,2)	0	0

the cylindrical function) sits between \hat{h}_{s_k} and $\hat{h}_{s_k}^{-1}$. But these two are the only non vanishing cases, for the following reason. The \hat{h} operators commute with each other and therefore we have to consider only the permutations of the three operator: \hat{V} , $\hat{O}_{(0)} = \hat{h}_{s_k} \hat{h}_{s_k}^{-1}$ and $\hat{O}_{(2)} = (\hat{h}_{\alpha_{ij}} - \hat{h}_{\alpha_{ji}})/2$. By the retracting identity, the $\hat{O}_{(0)}$ operator is a two-index operator in the spin 0 representation associated to the vertex v while the $\hat{O}_{(2)}$ operator is a two-index operator in the spin 1 representation associated to the same vertex v . But in the hamiltonian constraint there is a trace, and thus in all the orderings of the operators we have to take a trace in the representation associated to the vertex. The volume operator modifies only the recoupling in the vertex and not the representation associated to it. Therefore we will always have a trace between a spin 0 and a spin 1 representation, which gives zero. We can conclude that (4.17)

and (4.18) are the two only natural orderings for the HCO and their action reduces to the computation of equations (4.19) and (4.20).

Following Thiemann [22], we consider the *symmetric* euclidean HCO

$$\hat{\mathcal{H}}_{symm}^E[N] = \frac{1}{2} \left(\hat{\mathcal{H}}_\gamma^{E^{(1)}}[N] + \hat{\mathcal{H}}_\gamma^{E^{(1)}}[N]^\dagger \right). \quad (5.16)$$

Using the transformation properties of \hat{h} under conjugation, we have

$$\hat{\mathcal{H}}_{symm}^E[N] = \frac{1}{2} \left(\hat{\mathcal{H}}_\gamma^{E^{(1)}}[N] + \hat{\mathcal{H}}_\gamma^{E^{(2)}}[N] \right). \quad (5.17)$$

The coefficients A^s for the symmetric operators on trivalent vertices are

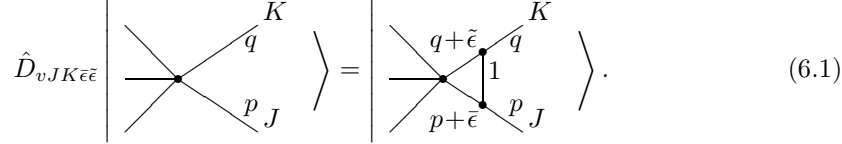
$$A^s(p, \bar{\epsilon}; q, \tilde{\epsilon}; r) = \frac{1}{3} \left[A^{(1)}(p, \bar{\epsilon}; q, \tilde{\epsilon}; r) + A^{(2)}(p, \bar{\epsilon}; q, \tilde{\epsilon}; r) \right] \quad (5.18)$$

In table 1 we give the values of $A^{(1)}$ and $A^{(2)}$ for the simplest 3-vertices.

6. Conclusions

We have computed matrix elements of Thiemann's euclidean hamiltonian constraint, for its two natural orderings. In particular we have computed the action of the operator on any trivalent vertex in closed algebraic form.

We collect here our results and express them in compact form. Following [45], we define the operator $\hat{D}_{vJK\bar{\epsilon}\tilde{\epsilon}}$ that acts on the vertex v by adding two new vertices on the edges J and K adjacent to v , and altering the colors of the two newly created edges by $\bar{\epsilon}, \tilde{\epsilon} = \pm 1$



$$\hat{D}_{vJK\bar{\epsilon}\tilde{\epsilon}} \left| \begin{array}{c} \text{Diagram of vertex } v \text{ with edges } p, q, r \end{array} \right\rangle = \left| \begin{array}{c} \text{Diagram of vertex } v \text{ with edges } p, q, r \text{ and new edges } q+\tilde{\epsilon}, p+\bar{\epsilon} \end{array} \right\rangle. \quad (6.1)$$

Using this operator, the action of Thiemann's HCO over a generic spin-network state is

$$\hat{\mathcal{H}}^E[N] \Psi_s = i l_0 \sum_{v \in \mathcal{V}(s)} N(x_v) \sum_{\substack{I, J, K \in \mathcal{E}(v) \\ \bar{\epsilon}, \tilde{\epsilon} = \pm 1}} \frac{1}{E(v)} \hat{A}_{vIJK\bar{\epsilon}\tilde{\epsilon}} \hat{D}_{vJK\bar{\epsilon}\tilde{\epsilon}} \Psi_s \quad (6.2)$$

where $\mathcal{V}(s)$ is the set of the vertices of s and $\mathcal{E}(v)$ is the set of the edges adjacent to v . In general, $\hat{A}_{vIJK\bar{\epsilon}\tilde{\epsilon}}$ are matrices in the finite dimensional space of the contractors at the vertex v , functions of the colors of the adjacent edges. On trivalent vertices, the space of these contractors has dimension one, and therefore the matrices $\hat{A}_{vIJK\bar{\epsilon}\tilde{\epsilon}}$ are numbers. Let s have trivalent gauge-invariant vertices only. Denote as (r, p, q) the colors associated to the edges I, J, K of a vertex v . Then

$$\begin{aligned} \hat{\mathcal{H}}^{E^{(1)}} \Psi_s &= \frac{2il_0}{3} \sum_{v \in \mathcal{V}(s)} \sum_{\bar{\epsilon} = \pm 1} \sum_{\tilde{\epsilon} = \pm 1} \left[A^{(1)}(p, \bar{\epsilon}; q, \tilde{\epsilon}; r) \hat{D}_{vJK\bar{\epsilon}\tilde{\epsilon}} \right. \\ &\quad \left. + A^{(1)}(q, \bar{\epsilon}; r, \tilde{\epsilon}; p) \hat{D}_{vKI\bar{\epsilon}\tilde{\epsilon}} + A^{(1)}(r, \bar{\epsilon}; p, \tilde{\epsilon}; q) \hat{D}_{vIJ\bar{\epsilon}\tilde{\epsilon}} \right] \Psi_s, \end{aligned} \quad (6.3)$$

where $i = 1, 2$ for the two orderings we have studied. The explicit values of the matrix elements $A^{(1)}(p, \bar{\epsilon}; q, \bar{\epsilon}; r)$ and $A^{(2)}(p, \bar{\epsilon}; q, \bar{\epsilon}; r)$ are

$$A^{(1)}(p, \bar{\epsilon}; q, \bar{\epsilon}; r) = \sum_{\epsilon=\pm 1} \frac{1}{4} \sqrt{w(p, q, r + \epsilon, 1)} R_1(r, \epsilon) R_2(p, \bar{\epsilon}; q, \bar{\epsilon}, r). \quad (6.4)$$

$$A^{(2)}(p, \bar{\epsilon}; q, \bar{\epsilon}; r) = \sum_{\epsilon=\pm 1} \frac{1}{4} \sqrt{w(p + \bar{\epsilon}, q + \bar{\epsilon}, r + \epsilon, 1)} R_1(r, \epsilon) R_2(p, \bar{\epsilon}; q, \bar{\epsilon}, r). \quad (6.5)$$

where $R_1(r, \epsilon)$, $R_2(p, \bar{\epsilon}; q, \bar{\epsilon}, r)$ and $w(a, b, c, 1)$ are explicitly given by (5.8) (5.9) and (A.17). We give some values of matrix elements in Table 1.

The technique we have used can be applied in a straightforward manner to vertices of any valence. The only limitation is given by the lack of an explicit algebraic formula corresponding to equations (A.11) and (A.17), for vertices of valence greater than four. The action of the volume operator is completely known; however, explicit values of its matrix elements are so far known throughout an algorithmic procedure [9] only. It is interesting to note that nothing in the action of the operator seems to depend on the continuous moduli studied in [46], which distinguish knots with high valence intersections. This might indicate that these parameters are superfluous and the theory lives actually in a smaller space. In this regard, see [47]. Finally, we expect that the technique used here can be applied to the second term in (4.7) as well, and therefore we expect that the total lorentzian hamiltonian constraint can be analyzed along the lines of this work.

Acknowledgments

We thank Thomas Thiemann for help in understanding his construction, Jurek Lewandowski for valuable discussions, criticisms and insights, Andreas Freund for pointing out a mistake in an earlier version of this work and Luca Lusanna for useful discussions on the quantization of constrained dynamical system. This work has been partially supported by the NSF grants PHY-9515506, PHY-90-12099, PHY-9514240 and PHY-5-3840400 and by the INFN grant “Iniziativa specifica FI-41”.

Appendix A. Explicit formulas for the volume operator.

As discussed in section 2.4, there exist two different versions of the volume operator [15]. They have the same action on generic trivalent vertices. The volume operator acts on a cylindrical function $\Psi_{\gamma, \psi}$ [13, 15, 43] by:

$$\begin{aligned} \hat{V} \Psi_{\gamma, \psi} &= l_0^3 \sum_{v \in \mathcal{V}(\gamma)} \hat{V}_v \Psi_{\gamma, \psi} = \left(l_0^3 \sum_{v \in V(\gamma)} \sqrt{\hat{V}^2} \right) \Psi_{\gamma, \psi} \\ &= \left(l_0^3 \sum_{v \in \mathcal{V}(\gamma)} \sqrt{\left| \frac{i}{16 \cdot 3!} \sum_{\mathbf{e}_I \cup \mathbf{e}_J \cup \mathbf{e}_K = v} \epsilon(\mathbf{e}_I, \mathbf{e}_J, \mathbf{e}_K) \hat{W}_{IJK} \right|} \right) \psi(g_1, \dots, g_N) , \end{aligned} \quad (A.1)$$

where, $\mathcal{V}(\gamma)$ is the set of all vertices of γ , $g_I = j_I(\bar{A}(\mathbf{e}_I))$, and $X_I = X(g_I)$ is the right invariant vector field on $SU(2)$. All edges are chosen as outgoing. Notice that the action of the operator is given as a sum over terms in which three edges are “grasped” namely acted upon by one of the left-invariant vector fields.

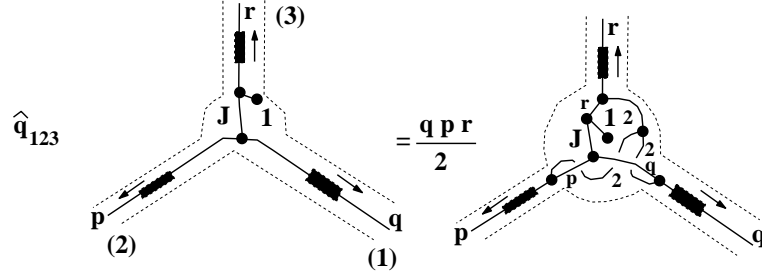


Figure A1. Graphical representation of the grasping of the volume operator in the case of a gauge non-invariant 3-valent vertex.

Here $\epsilon(\mathbf{e}_I, \mathbf{e}_J, \mathbf{e}_K) = \text{sgn}(\det(\dot{e}_I(0), \dot{e}_J(0), \dot{e}_K(0)))$ and we have defined

$$\hat{W}_{IJK} = 2 \epsilon_{ijk} X_I^i X_J^j X_K^k. \quad (\text{A.2})$$

(\hat{q} in [13, 43] is related to \hat{W} in [9] by $\hat{W}_{[IJK]} = 2 \hat{q}_{IJK}$.) As noted in [15], the difference between the volume introduced by Rovelli and Smolin in [11] and the one later introduced by Ashtekar and Lewandowski [13] is given by

$$\hat{V}_{\text{RS}}^2 = \frac{1}{3!} \sum_{\mathbf{e}_I \cup \mathbf{e}_J \cup \mathbf{e}_K = v} \left| \frac{i}{16} \hat{W}_{[IJK]} \right|, \quad (\text{A.3})$$

$$\hat{V}_{\text{AL}}^2 = \left| \frac{i}{16} \frac{1}{3!} \sum_{\mathbf{e}_I \cup \mathbf{e}_J \cup \mathbf{e}_K = v} \epsilon(\mathbf{e}_I, \mathbf{e}_J, \mathbf{e}_K) \hat{W}_{[IJK]} \right|. \quad (\text{A.4})$$

This difference is due to a different regularization procedure used to derive the operator from its classical expression. From equations (A.4) and (A.3) it follows that the action of the two operators coincides when evaluated on generic (non coplanar) trivalent vertices, since there is only one term in the sum.

Notice that the action of this operator is defined on gauge non-invariant states as well, since it is defined only in terms of left invariant vector field and therefore over the whole $\bar{\mathcal{A}}$ space. Furthermore, explicit inspection of the definition of the operator shows that its action on a gauge non-invariant n -valent vertex coincides with one of the terms of its action on an $(n+1)$ -valent vertex.

To see this, consider the action of the volume on a 3-valent gauge non-invariant vertex in which the three colors of the adjacent edges are p, q, r , the color of the representation at the vertex is t , and the intertwiner is c . And consider the action of the volume on a gauge-invariant 4-valent vertex with edges colored p, q, r, t and intertwiner c . The latter is given by the sum of four terms. In one of these four terms, the three left invariant vector fields in (A.2) grasp the three edges colored p, q, r . It is obvious that the resulting algebra is precisely the same as the one of the single term in the action of the volume on the trivalent gauge non-invariant vertex.

Using this, we have, in graphical form, the key result on which the computations of this paper are based::

$$\hat{W}_{[012]} \begin{array}{c} p \\ \diagup \\ \text{---} J \text{---} \\ \diagdown \\ q \end{array} \begin{array}{c} r \\ \diagup \\ \text{---} t \text{---} \\ \diagdown \end{array} = \sum_I W_{[012]}^{(4)J^I}(q, p, r, t) \begin{array}{c} p \\ \diagup \\ \text{---} I \text{---} \\ \diagdown \\ q \end{array} \begin{array}{c} r \\ \diagup \\ \text{---} t \text{---} \\ \diagdown \end{array}, \quad (\text{A.5})$$

where we have indicated by $[012]$ the triple of edges colored q, p and r . In the computations in the text, we have the particular case in which r is $r \pm 1$ and $t = 1$. We write

$$\hat{W}_{[012]} |v_J\rangle = \sum_I W_{[012]}^{(4)J^I}(q, p, r \pm 1, 1) |v_I\rangle. \quad (\text{A.6})$$

where $|v_I\rangle$ is a compact notation for the vertex with internal edge colored I . $W_{[012]}^{(4)J^I}$ was explicitly computed in [9] in terms of 9- j and 6- j symbols:

$$\begin{aligned} W_{[012]}^{(4)J^I}(q, p, r \pm 1, 1) &= \frac{q \, p \, (r \pm 1) \, \Delta_I \left\{ \begin{matrix} q & p & I \\ q & p & J \\ 2 & 2 & 2 \end{matrix} \right\} \text{ Tet} \left[\begin{matrix} J & I & 1 \\ r \pm 1 & r \pm 1 & 2 \end{matrix} \right]}{\theta(q, p, I) \theta(r \pm 1, 1, I) \theta(2, J, I)} = \\ &= q \, p \, (r \pm 1) \frac{\text{Diagram 1}}{\text{Diagram 2}} \text{Diagram 3} \end{aligned} \quad (\text{A.7})$$

This is the action on non-normalized states. Inserting the vertex normalization (equation (7.28) of [9]) we get:

$$\hat{W}_{[012]} \sqrt{\frac{\text{Diagram 1}}{\text{Diagram 2}}} |v_J\rangle_N = \sum_I i W_{[012]}^{(4)J^I}(p, q, r \pm 1, 1) \sqrt{\frac{\text{Diagram 1}}{\text{Diagram 2}}} |v_I\rangle_N.$$

Thus we can write the action of the (square of the) volume operator on the normalized states as

$$\hat{W}_{[012]} |v_J\rangle_N = \sum_I i \widetilde{W}_{[012]}^{(4)J^I}(p, q, r \pm 1, 1) |v_I\rangle_N, \quad (\text{A.8})$$

where $\widetilde{W}_{[012]}^{(4)J^I}(p, q, r \pm 1, 1)$ are the matrix elements of the $\hat{W}_{[012]}$ vertex operator in the normalized basis. Their values are explicitly given by:

$$\begin{aligned} \widetilde{W}_{[012]}^{(4)J^I}(p, q, r \pm 1, 1) &= \\ &= q \, p \, (r \pm 1) \sqrt{\frac{\text{Diagram 1}}{\text{Diagram 2}}} \text{Diagram 3} \end{aligned} \quad (\text{A.9})$$

In this form it is obvious that $\widetilde{W}_{[012]}^{(4)J^I}(p, q, r \pm 1, 1)$ is symmetric in I and J .

An important observation is that I and J can take only two values in order to be compatible with $r \pm 1$ and 1 at the triple intersection; these are r and $r + 2$ for the $(+)$ case; and r and $r - 2$ in the $(-)$ case. But since the diagonal entries of \widetilde{W}_J^I are zero, there is only one possibility, which is $I = r \pm 2$. Thus the eigenvalues of the 2×2 matrix \widetilde{W} are $\pm i w(q, p, r \pm 1, 1)$ with

$$w(p, q, r \pm 1, 1) = \sqrt{\left| \widetilde{W}_{[012]}^{(4)r \pm 2}(p, q, r \pm 1, 1) \right|} \quad (\text{A.10})$$

From the eigenvalues of the W matrices we immediately obtain the eigenvalues of the volume operator. In fact, since the W matrix is a 2×2 antisymmetric matrix, its absolute value is a multiple of the identity. Thus the volume acts diagonally in the case in which we are interested, much simplifying the calculations. Taking the square root of the absolute value yields

$$\hat{V}_v \left| \begin{array}{c} p \\ \diagdown \\ \bullet \\ \diagup \\ q \end{array} \begin{array}{c} J \\ \text{---} \\ 1 \\ \bullet \end{array} \begin{array}{c} r_{\pm 1} \end{array} \right\rangle = \frac{l_0^3}{4} \sqrt{w(q, p, r_{\pm 1}, 1)} \left| \begin{array}{c} p \\ \diagdown \\ \bullet \\ \diagup \\ q \end{array} \begin{array}{c} J \\ \text{---} \\ 1 \\ \bullet \end{array} \begin{array}{c} r_{\pm 1} \end{array} \right\rangle \quad (\text{A.11})$$

Let us compute the values of w . Starting from equation (A.9) the matrix elements of $\tilde{W}_{[012]}^{(4)} J^I$ are given by the chromatic evaluation:

$$\widetilde{W}_{[012]}^{(4)}(a, b, c, d)_{J^I} = a b c \sqrt{\frac{\text{Diagram 1}}{\text{Diagram 2}}} \quad (\text{A.12})$$

where the matrices $\widetilde{W}_{[012]}^{(4)}(a, b, c, d)_J^I$ are real antisymmetric matrices and have elements different from zero only if $|J - I| = 2$. Using equation (C.9) and applying (C.11) to the two vertices $v(a, 2, a)$, $v(a, b, I)$ we obtain:

$$\begin{aligned} \widetilde{W}_{[012]}^{(4)}(a, b, c, d)_{J^I} = & \sqrt{\frac{\text{Diagram 1}}{\text{Diagram 2}}} \cdot \text{Diagram 3} \times \quad (\text{A.13}) \\ & \times \left[b \frac{\text{Diagram 4}}{\text{Diagram 5}} - I \frac{\text{Diagram 6}}{\text{Diagram 7}} \right] \cdot \left[b \frac{\text{Diagram 8}}{\text{Diagram 9}} \right] \cdot \left[c \frac{\text{Diagram 10}}{\text{Diagram 11}} \right] \end{aligned}$$

This expression is evaluated using (C.12),(C.13) and (C.14). Defining $t = (I - J)/2$ and $\epsilon = (I + J)/2$ we note that $\bar{W}_{[012]}^{(4)}(a, b, c, d)J^I$ is different from zero only if $\epsilon = \pm 1$ and all the 3-vertices in equation (A.13) are admissible. In this way, we obtain the following explicit formula for the matrix elements ($\epsilon = \pm 1$):

$$\begin{aligned} \widetilde{W}_{[012]}^{(4)}(a, b, c, d)_{t-\epsilon}^{t+\epsilon} = & -\epsilon(-1)^{\frac{a+b+c+d}{2}} \left[\frac{1}{4t(t+2)} \frac{a+b+t+3}{2} \frac{c+d+t+3}{2} \right. \\ & \frac{1+a+b-t}{2} \frac{1+a+t-b}{2} \frac{1+b+t-a}{2} \\ & \left. \frac{1+c+d-t}{2} \frac{1+c+t-d}{2} \frac{1+d+t-c}{2} \right]^{\frac{1}{2}} \end{aligned} \quad (\text{A.14})$$

This formula can be used to obtain explicit expressions for the eigenvalues of the $|\hat{W}_{[012]}^{(4)}(a, b, c, d)|$ operator when they are 2×2 matrices, as in the case of equation (A.11),

$$w(a, a, 1, 1) = \sqrt{\frac{a(a+2)}{4}} \quad (\text{A.15})$$

$$w(a, b, c, a + b + c - 2) = 2\sqrt{\frac{a b c (a + b + c)}{16}} \quad (\text{A.16})$$

$$w(a, b, c, 1) = \frac{1}{2}\sqrt{\frac{(a + b + c + 3)(1 + a + b - c)(1 + c - a + b)(1 + c + a - b)}{16}} \quad (\text{A.17})$$

Appendix B. Graphical calculus in the connection representation.

Let us recall the basic elements of Penrose binor calculus [44], which is the basis for expressing the cylindrical functions of generalized connections in graphical form [37]. The key idea of Penrose is to rewrite any tensor expression in which there are sums of dummy indices in a graphical way [44]. Penrose represents the basic elements of spinor calculus (i.e., tensor expression with indices $A, B, \dots = 1, 2$) as

$$\begin{aligned} \delta_C^A &= \begin{array}{c} \bullet^A \\ | \\ \bullet_C \end{array} & i\epsilon_{AC} &= \begin{array}{c} \bullet^A \\ \curvearrowright \\ \bullet_C \end{array} & i\epsilon^{AC} &= \begin{array}{c} \bullet^A \\ \curvearrowleft \\ \bullet_C \end{array} \\ \eta_A &= \begin{array}{c} \boxed{\eta} \\ \bullet_A \end{array} & \eta^A &= \begin{array}{c} \bullet^A \\ \boxed{\eta} \end{array} & X_{AB}^C &= \begin{array}{c} \bullet^C \\ \boxed{X} \\ \bullet_A \bullet_B \end{array} \end{aligned} \quad (\text{B.1})$$

and assigns a minus sign to each crossing[†], i.e:

$$X_{CD}^{AB} = \delta_D^A \delta_C^B = - \begin{array}{c} \bullet^A \bullet^B \\ \times \\ \bullet_C \bullet_D \end{array} \quad (\text{B.2})$$

Using this rule it is possible to represent any $SU(2)$ tensor expression in a graphical way as follows: **(1)** Define the “up” direction in the plane; **(2)** Draw boxes with the name of the $SU(2)$ tensor (except for the δ and the ϵ that are simply represented by lines) with as many slots going up as the number of contravariant indices and as many slots going down as the number of covariant indices; **(3)** For each dummy index connect with a line the corresponding slots of the boxes; **(4)** Assign a “i” factor to each minimum or maximum of the lines; **(5)** Assign a minus sign to each crossings of lines. Conversely, any curve can expressed as a product of δ ’s and ϵ ’s.

An unexpected feature of this graphical calculus is its way of expressing the operation of taking the trace. Since any contravariant index of a tensor is represented more “up” than any covariant index of the same tensor, there is no way to write directly the operation of taking the trace unless one uses the antisymmetric 2-tensors ϵ_{AB} and ϵ^{AB} as $\text{Tr} X_B^A = X_B^A \delta_A^B = \epsilon_{A'A} \epsilon^{B'B} X_B^A \delta_{B'}^{A'}$. This becomes, graphically,

$$\text{Tr} X_B^A = \delta_A^B X_B^A = - \begin{array}{c} \boxed{X} \end{array} \quad (\text{B.3})$$

Moreover, the basic binor identity is graphically given by

$$\begin{array}{c} \times \\ + \\ | \\ + \\ \cup \end{array} = (-1) \delta_B^C \delta_A^D + \delta_A^C \delta_B^D + (-1) \epsilon_{AB} \epsilon^{CD} = 0, \quad (\text{B.4})$$

perhaps the most relevant equation of loop quantum gravity.

In particular, the irreducible representation of color n can be constructed as the symmetrization $\Pi_n^{(e)}$ (in Penrose’s graphical representation an anti-symmetrization because of equation (B.2)) of the tensor product of n fundamental representations $\begin{array}{c} \boxed{\eta} \\ \bullet_A \end{array}^B = U(g)_A^B$ (g being the group element). Denoting by $\Pi_n^{(e)}$ the normalized

[†] The binor representation is a graphical representation in the plane.

symmetrizer (graphically an anti-symmetrizer – see [37]), the color n irreducible representation is given by:

$$\Pi_n^{(e)} P_n = \frac{1}{n!} \sum_p (-1)^{|p|} P_n^{(p)} = \begin{array}{c} |n \\ \hline \text{---} \\ | \end{array} \quad (\text{B.5})$$

$$J_I(n_I) = \begin{array}{c} |n_I \\ \hline \text{---} \\ | \end{array} \mathbf{e}_I = \begin{array}{c} |n_I \\ \hline \boxed{g_{e_I} \cdots g_{e_I}} \\ \hline |n_I \end{array}, \quad (\text{B.6})$$

(P_n represents n parallel lines, $P_n^{(p)}$ is the graphical representation in terms of lines of the permutation p , $|p|$ is the parity of the permutation and a line labeled by a positive integer n represents n non-intersecting parallel line).

Analogously, it is possible to construct an explicit graphical representation of the Clebsch-Gordan intertwining matrix i.e., of the matrix that represents the coupling of 3 (or more) irreducible representations of the $SU(2)$ group. The representation of the Clebsch-Gordan intertwining matrix in the binor formalism is given by the special sum of “tangles” denoted as the 3-vertex. Each line of the vertex is labeled by a positive integer a , b or c and is defined as:

$$\begin{array}{c} a \quad b \\ \diagdown \quad \diagup \\ |c \end{array} \stackrel{\text{def}}{=} \begin{array}{c} a \quad m \\ \diagdown \quad \diagup \\ |p \quad \text{---} \quad |n \\ \diagup \quad \diagdown \\ |c \end{array} \quad \left\{ \begin{array}{l} m = (a+b-c)/2 \\ n = (b+c-a)/2 \\ p = (c+a-b)/2 \end{array} \right. \quad (\text{B.7})$$

where m, n, p are positive integers. This last condition is called the *admissibility condition* for the 3-vertex. By the Wigner-Eckart theorem, or more precisely, by the version of it due to Yutsin, Levinson and Vanagas [48], any invariant tensorial intertwining matrix representing the coupling of n representations of a compact group can be expressed as the product of Clebsch-Gordan coefficients or, which is the same, in terms of a trivalent decomposition. It is easy to see that any contractor c_α of a given vertex v_α with n incoming (outgoing) edges of color P_0, \dots, P_{n-1} , can be written in terms of a linear combination of the trivalent contractors obtained ordering the edges and assigning $n-3$ compatible integers, i.e. by a trivalent decomposition of the vertex. Graphically:

$$\begin{array}{c} P_2 \quad \cdots \quad P_{n-3} \\ \diagdown \quad \cdots \quad \diagup \\ |c_\alpha \\ \diagup \quad \cdots \quad \diagdown \\ P_1 \quad \text{---} \quad P_{n-2} \\ \diagdown \quad \cdots \quad \diagup \\ P_0 \quad \text{---} \quad P_{n-1} \end{array} = \sum_{i_2, \dots, i_{n-2}} c(i_2, \dots, i_{n-2}) \begin{array}{c} P_2 \quad \cdots \quad P_{n-3} \\ \diagdown \quad \cdots \quad \diagup \\ |i_2 \quad \text{---} \quad |i_3 \quad \cdots \quad |i_{n-2} \\ \diagup \quad \cdots \quad \diagdown \\ P_1 \quad \text{---} \quad P_{n-2} \\ \diagdown \quad \cdots \quad \diagup \\ P_0 \quad \text{---} \quad P_{n-1} \end{array}, \quad (\text{B.8})$$

where the sum is extended to all the integers i_2, \dots, i_{n-2} that satisfy the *admissibility conditions* for the 3-vertices.

An important characteristic of the binor representation, related to the existence of the natural “metric” (an invariant way to relate contravariant and covariant indices) ϵ_{AB} in the 2-spinor space, it is its independence from the orientation chosen for the edges. In fact, the $SU(2)$ relation $U(g^{-1})^B_A = \epsilon_{AC} \epsilon^{BD} U(g)^C_D$ is graphically represented (in the binor representation) by:

$$\begin{array}{c} |A \\ \boxed{X^{-1}} \\ |B \end{array} = \begin{array}{c} |A \\ \boxed{g} \\ |g \end{array}, \quad \text{while} \quad \begin{array}{c} |n_i \\ \text{---} \\ | \end{array} \mathbf{e}_i^{-1} = \begin{array}{c} | \text{---} \\ \boxed{\mathbf{e}_i} \\ |n_i \end{array}. \quad (\text{B.9})$$

is the related identity in case of the n -representation.

In this graphical notation the left invariant vector fields associate to an edge are represented by:

$$X_{\mathbf{e}_I}^i \text{ (edge with } n_I \text{ framing)} = n_I \text{ (edge with } n_I \text{ framing and a loop labeled } i \text{)} \quad (\text{B.10})$$

From the identity (that can be proven in a straightforward way):

$$\sum_{i,j,k=1}^3 \epsilon_{ijk} \text{ (three edges with framing 2 and loops } i, j, k \text{)} = \frac{1}{2} \text{ (three edges with framing 2)} \quad (\text{B.11})$$

we have the important result

$$\epsilon_{ijk} X_{\mathbf{e}_I}^i X_{\mathbf{e}_J}^j X_{\mathbf{e}_K}^k \text{ (three edges with framing } n_I, n_J, n_K \text{)} = \frac{n_I n_J n_K}{2} \text{ (three edges with framing } n_I, n_J, n_K \text{ and a loop)} \quad (\text{B.12})$$

which is the key “bridge” showing that the volume operator that was defined in the loop representation in [11], based on the r.h.s. of (B.12), is indeed the same operation as the volume that was defined in the connection representation in [13], based on the l.h.s. of (B.12).

Appendix C. Tangle-theoretic recoupling theory.

One of the main results of the recoupling theory of colored knots and links with trivalent vertices [31] is the computation of the Kauffman bracket for framed spin networks. The framing refers to the fact that in the computations one keeps track of over- and under-crossing. In our context this distinction has no meaning. Therefore we use a simplified version of the recoupling theory, namely we replace the deformation parameter A by its “classical” value -1 , relevant to our case. This case corresponds to the standard recoupling theory of the $SU(2)$ group. In the formulae from [31], we thus replace the deformed (or quantum) integers by ordinary integers. We list here the basic formulae which we use. For more details see [31]. This beauty of the theory is that it is completely determined by the following two tangle properties:

$$\langle \text{crossing} \rangle = A \langle \text{cup} \rangle + A^{-1} \langle \text{cap} \rangle, \quad (\text{C.1})$$

$$\langle \text{loop} \cup \mathbf{K} \rangle = d \langle \mathbf{K} \rangle, \quad (\text{C.2})$$

where $d = -A^2 - A^{-2}$ and \mathbf{K} is any diagram that does not intersect the added loop. The graphical representation of the states that we have defined in section 3 does satisfy these two equations (with $A = -1$) and therefore all recoupling theory equations can be applied.

There is a subtle point that needs to be clarified here. When tangle theoretical recoupling theory is defined on a pane, it corresponds, via Penrose binor calculus to the

(1) The symmetrizer

(2) The θ net

where $m = (a + b - c)/2$, $n = (b + c - a)/2$, $p = (c + a - b)/2$.

(3) The Tetrahedral net

where

$$\begin{aligned} a_1 &= \frac{A+D+E}{2}, & b_1 &= \frac{B+D+E+F}{2}, \\ a_2 &= \frac{B+C+E}{2}, & b_2 &= \frac{A+C+E+F}{2}, \\ a_3 &= \frac{A+B+F}{2}, & b_3 &= \frac{A+B+C+D}{2}, \\ a_4 &= \frac{C+D+F}{2}, \\ m &= \max\{a_i\}, & M &= \min\{b_j\}, \\ \mathcal{E} &= A!B!C!D!E!F!, & \mathcal{I} &= \prod_{ij} (b_j - a_i)! . \end{aligned}$$

The most important result of the theory is the recoupling theorem which states:

$$\begin{array}{c} b \\ \diagdown \\ \bullet \\ \diagup \\ a \end{array} \begin{array}{c} j \\ \bullet \\ \diagup \\ \bullet \\ \diagdown \\ d \end{array} \begin{array}{c} c \\ \diagup \\ \bullet \\ \diagdown \\ d \end{array} = \sum_i \left\{ \begin{array}{ccc} a & b & i \\ c & d & j \end{array} \right\} \begin{array}{c} b \\ \diagdown \\ \bullet \\ \diagup \\ a \end{array} \begin{array}{c} i \\ \bullet \\ \diagup \\ \bullet \\ \diagdown \\ d \end{array} \begin{array}{c} c \\ \diagup \\ \bullet \\ \diagdown \\ d \end{array} \quad (\text{C.6})$$

where the quantities $\left\{ \begin{array}{ccc} a & b & i \\ c & d & j \end{array} \right\}$ are the $su(2)$ 6- j symbols (normalized as in [31]) and their explicit values, in terms of chromatic evaluations, are:

$$\left\{ \begin{array}{ccc} a & b & i \\ c & d & j \end{array} \right\} = \frac{\Delta_i \text{Tet} \left[\begin{array}{ccc} a & b & i \\ c & d & j \end{array} \right]}{\theta(a, d, i) \theta(b, c, i)}. \quad (\text{C.7})$$

From the previous formulae and definitions other relations can be easily derived. In particular, exchanging the ordering of the three line in a 3-vertex yields a sign factor:

$$\begin{array}{c} a \\ \diagdown \\ \bullet \\ \diagup \\ c \end{array} \begin{array}{c} b \\ \diagup \\ \bullet \\ \diagdown \\ c \end{array} = \lambda_c^{ab} \begin{array}{c} a \\ \diagdown \\ \bullet \\ \diagup \\ c \end{array} \begin{array}{c} b \\ \diagup \\ \bullet \\ \diagdown \\ c \end{array} \quad (\text{C.8})$$

where $\lambda_c^{ab} = (-1)^{(a+b-c)/2} (-1)^{(a'+b'-c')/2}$, and $x' = x(x+2)$; The following reduction holds

$$\begin{array}{c} k \\ \bullet \\ a \\ \bullet \\ i \end{array} \begin{array}{c} c \\ \bullet \\ d \\ \bullet \\ c \end{array} = \frac{\begin{array}{c} k \\ \bullet \\ a \\ \bullet \\ i \end{array} \begin{array}{c} c \\ \bullet \\ d \\ \bullet \\ c \end{array}}{\begin{array}{c} k \\ \bullet \\ a \\ \bullet \\ i \end{array}} \cdot \begin{array}{c} k \\ \bullet \\ a \\ \bullet \\ i \end{array} \quad (\text{C.9})$$

Another key formula that can be derived is the one we use for evaluating the action of the parallel propagator operator on spin network states:

$$\left| \begin{array}{c} n \\ 1 \end{array} \right| = \sum_{\epsilon=\pm 1} a_\epsilon(n) \left| \begin{array}{c} n \\ n+\epsilon \\ n \end{array} \right|_1 = \left| \begin{array}{c} n \\ n+1 \\ n \end{array} \right|_1 + \frac{\Delta_{n-1}}{\Delta_n} \left| \begin{array}{c} n \\ n-1 \\ n \end{array} \right|_1. \quad (\text{C.10})$$

Also

$$r \cdot \begin{array}{c} p \\ \diagdown \\ 2 \\ \bullet \\ r \end{array} \begin{array}{c} q \\ \diagup \\ \bullet \\ \diagdown \\ r \end{array} = p \cdot \begin{array}{c} p \\ \diagdown \\ 2 \\ \bullet \\ r \end{array} \begin{array}{c} q \\ \diagup \\ \bullet \\ \diagdown \\ r \end{array} + q \cdot \begin{array}{c} p \\ \diagdown \\ 2 \\ \bullet \\ r \end{array} \begin{array}{c} q \\ \diagup \\ \bullet \\ \diagdown \\ r \end{array} \quad (\text{C.11})$$

Finally, using equations (C.6) and (C.7), we have the chromatic evaluations ($\epsilon = 0, \pm 1$)

$$(t+\epsilon) \cdot \frac{\begin{array}{c} t+\epsilon \\ \bullet \\ 2 \\ \bullet \\ t+\epsilon \end{array} \begin{array}{c} 2 \\ \bullet \\ 2 \\ \bullet \\ 2 \end{array}}{\begin{array}{c} 2 \\ \bullet \\ t+\epsilon \\ \bullet \\ t-\epsilon \end{array}} = -1 - \epsilon \left[\frac{t+1}{2} \right] \quad (\text{C.12})$$

$$b \cdot \begin{array}{c} \text{---} t+1 \text{---} \\ \diagup \quad \diagdown \\ \text{---} 2 \text{---} \\ \diagdown \quad \diagup \\ \text{---} t-1 \text{---} \end{array} \begin{array}{c} b \\ b \\ b \end{array} a = \frac{1+a+b-t}{2} \cdot \begin{array}{c} a \\ \text{---} b \text{---} \\ t+1 \end{array} \quad (\text{C.13})$$

$$\frac{\begin{array}{c} a \\ \text{---} b \text{---} \\ t+1 \end{array}}{\begin{array}{c} a \\ \text{---} b \text{---} \\ t-1 \end{array}} = - \frac{(3+a+b+t)(1+a+t-b)(1+b+t-a)}{4t(t+1)(1+a+b-t)} \quad (\text{C.14})$$

These formulas are sufficient for the computations in the paper.

References

- [1] Dirac P A M 1958 *Proc. R. Soc. London*, **A246**, 333;
Arnowitt R, Deser S and Misner C 1962 in *Gravitation: An Introduction to Current Research*, ed L. Witten, (Wiley, New York, 1962).
- [2] DeWitt B S 1967 *Phys. Rev. D* **160** 1113;
Wheeler J A 1968, in *Battelle rencontres 1967* ed. C DeWitt and J A Wheeler (Benjamin, New York).
- [3] C Rovelli and L Smolin 1988 *Phys. Rev. Lett.* **61** 1155;
—1990 *Nucl. Phys.* **B331**, 80.
- [4] Sen A 1982 *Phys. Lett.* **119B** 89.
- [5] Ashtekar A 1986 *Phys. Rev. Lett.* **57** 2244;
—1987 *Phys. Rev.* **D36** 1587;
Rovelli C 1991 *Class. Quantum Grav.* **8**, 1613.
- [6] Barbero J F 1995 *Phys. Rev.* **D51**, 5498;
—1995 *Phys. Rev. D* **51** 5507.
- [7] Thiemann T 1996 *Class. Quantum Grav.* **13** 1383;
Ashtekar A 1996 *Phys. Rev. D* **53** 2865;
Loll R 1996 *Phys. Rev. D* **54** 5381;
Immizzi G 1996 *Class. Quantum Grav.* **13** 2385;
—1996 “Real and Complex Connections for Canonical Gravity” *xxx-archive* gr-qc/9612030.
- [8] Rovelli C 1996 “Loop Quantum Gravity and Black hole Physics”, *Helv. Phys. Acta* **69** 582.
- [9] De Pietri R and Rovelli C 1996 *Phys. Rev. D* **54** 2664.
- [10] Baez JC 1994 *Knots and Quantum Gravity* (Oxford University Press);
Ehlers J and Friedrich H 1995 *Canonical Gravity: From Classical to Quantum* Lectures Notes in Physics 434 (Springer Verlag, Berlin);
Ashtekar A 1995, in *Gravitation and Quantization, Les Houches, Session LVII*, ed B. Julia and J. Zinn-Justin (Elsevier Science);
Gambini R and Pullin J 1996 *Loops, Knots, Gauge Theories and Quantum Gravity* (Cambridge University Press).
- [11] Rovelli C and Smolin L 1995 *Nucl. Phys.* **B442**, 593; Erratum: *Nucl. Phys.* **B456** 734.
- [12] Loll R 1995 *Phys. Rev. Lett.* **75** 3048;
—1995 *Nucl. Phys.* **B444**, 619;
—1996 *Nucl. Phys.* **B460**, 143.
- [13] Lewandowski J 1994 *Int. J. Mod. Phys.* **D3**, 207-210
Lewandowski 1995 “The Operators of Quantum Gravity”, lecture given at the *Workshop on Canonical Quantum Gravity* Warsaw;
Ashtekar A and Lewandowski J 1995, *J. Geom. Phys.* **17** 191.
- [14] Lehner L, Frittelli S and Rovelli C 1996 *Class. Quantum Grav.* **13**, 2921.
- [15] Lewandowski J 1997 *Class. Quantum Grav.* **14**, 71.
- [16] Rovelli C 1993 *Nucl. Phys.* **B405**, 797;
—1993 *Phys. Rev.* **D47**, 1703.
- [17] Jacobson T and Smolin L 1988 *Nucl. Phys.* **B299**, 295.
- [18] Husain V 1988 *Nucl. Phys.* **B313** 711;

- Blencowe MP 1990 *Nucl. Phys.* **B341** 213;
 Brüggman B and Pullin J 1991 *Nucl. Phys.* **B363**, 221;
 Brüggman B, Gambini R and Pullin J 1992 *Phys. Rev. Lett.* **68**, 431;
 ———1992 *Nucl. Phys.* **B385** 587;
 ———1993 *Gen. Rel. and Grav.* **25**, 1;
 Pullin J 1993, in *Proceedings of the Vth Mexican School of Particles and Fields* edited by J Lucio (World Scientific, Singapore);
 Gambini R and Pullin J 1994, in in *Knots and quantum gravity*, J. Baez (ed), (Oxford University Press, Oxford 1994);
 ———1996 *xxx-archive Phys. Rev.* **D54** 5935;
 ———1996 *xxx-archive Class. Quantum Grav.* **13** L125;
 Borissov R 1997 *Phys. Rev.* **D55** 2059
- [19] Rovelli C and Smolin L 1994 *Phys. Rev. Lett.* **72**, 446.
 [20] Borissov R 1996 “Graphical Evolution of Spin Network States”, *xxx-archive* gr-qc/9606013, to appear on *Phys. Rev. D*.
 [21] Ezawa K 1996, *xxx-archive* gr-qc/9601050.
 [22] T Thiemann 1996 *Phys. Lett.* **B380**, 257;
 ———1996 “Quantum Spin Dynamics (QSD)”, *xxx-archive* gr-qc/9606089;
 ———1996 “Quantum Spin Dynamics (QSD) II”, *xxx-archive* gr-qc/9606090.
 [23] Gambini R and Pullin J 1997 “Chern–Simons states in spin-network quantum gravity” *xxx-archives* gr-qc/9703042.
 [24] Reisenberger M P and Rovelli C 1996 “Sum over Surfaces form of Loop Quantum Gravity”, *xxx-archive* gr-qc/9612045.
 [25] Markopoulos F and Smolin L 1997 “Causal evolution of spin networks” *xxx-archive* gr-qc/9702025;
 Baez J 1997, Seminar at Penn State University.
 [26] Smolin L 1996 “The classical limit and the form of the hamiltonian constraint in nonperturbative quantum general relativity”, *xxx-archive* gr-qc/9609034.
 [27] Rovelli C and Smolin L 1995 *Phys. Rev.* **D53**, 5743.
 [28] Lewandowski J 1994, *Int. J. Mod. Phys.* **D3**, 207.
 [29] Baez J C 1994 *Lett. Math. Phys.* **31**, 213;
 ———1994 in *Proceedings of the Conference on Quantum Topology*, edited by D. N. Yetter (World Scientific, Singapore, 1994);
 ———1996 *Adv. Math.* **117**, 253;
 ———1996 in *The Interface of Knots and Physics*, edited by Kauffman L H (American Mathematical Society, Providence, Rhode Island, 1996).
- [30] Smolin Lee 1997 “The future of spin networks”, *xxx-archive* gr-qc/9702030.
 [31] Kauffman L H and Lins S L 1994 *Temperley-Lieb Recoupling Theory and Invariants of 3-Manifolds* (Princeton University Press, Princeton NJ, 1994).
 [32] Major S and Smolin L 1996 *Nucl. Phys.* **B473** 267.
 Borissov R, Major S and Smolin L 1996 *Class. Quantum Grav.* **13** 3183;
 [33] Thiemann T 1995 *Acta Cosmologica* **XXI-2**, 145;
 ———1996, “The inverse loop transform” *xxx archive* gr-qc/9601105.
 [34] Ashtekar A and Lewandowski J 1996 *Class. Quantum Grav.* **14**, A55.
 [35] Ashtekar A and Isham C J 1992 *Class. Quantum Grav.* **9**, 1433.
 [36] Ashtekar A and Lewandowski J 1995, “Representation theory of analytic holonomy C^* algebras”, in *Knots and quantum gravity*, J. Baez (ed), (Oxford University Press, Oxford 1994);
 ———1995, *J. Math. Phys.* **36**, 2170.
 [37] De Pietri R 1997, *Class. Quantum Grav.* **14**, 53.
 [38] Marolf D 1997, personal communication.
 [39] Glimm J and Jaffe A 1987, *Quantum Physics*, (Springer Verlag, New York).
 [40] Baez J 1994, *Lett. Math. Phys.* **31**, 213;
 ———1994, “Diffeomorphism invariant generalized measures on the space of connections modulo gauge transformations”, *xxx-archive* hep-th/9305045, in the Proceedings of the conference on quantum topology, Yetter D (ed) (World Scientific, Singapore, 1994).
 [41] Marolf D and Mourão J M 1995 *Commun. Math. Phys.* **170**, 583.
 [42] Loll R 1993 *Nucl. Phys.* **B400**, 126.
 [43] Thiemann T 1996, “Closed formula for the matrix elements of the volume operator in canonical quantum gravity” *xxx-archive* gr-qc/9606091.
 [44] Penrose R 1971, in *Quantum Theory and Beyond*, edited by Bastin T (Cambridge University Press, Cambridge, 1971);

- 1971, in *Combinatorial Mathematics and its Application*, edited by Welsh D (Academic Press, New York, 1971);
- Kauffman L H 1990 *Inter. Journ. of Modern Physics A* **5**, 417;
- Moussoris J P 1979, in *Advances in Twistor Theory, Research Notes in Mathematics*, edited by L P Hughston and R S Ward (Pitman, 1979), pp. 308–312.
- [45] C Rovelli 1995 *J. Math. Phys.* **36** 6529.
- [46] Grott N and Rovelli C 1996 *J. Math. Phys.* **37** 3014.
- [47] Zapata JA 1997 “A Combinatorial Approach to Diffeomorphism Invariant Quantum Gauge Theories” *xxx-archive* gr-qc/9703037.
- [48] Yutsin A P, Levinson J B, and Vanagas V V 1962, *Mathematical Apparatus of the Theory of Angular Momentum* (Israel program for Scientific Translation, Jerusalem, 1962);
- Brink D M and Satchler R 1968, *Angular Momentum* (Claredon Press, Oxford, 1968);
- Citanović P 1984, *Group theory* (Nordita classical illustrated, Copenhagen , 1984).